Viscuit and the fluctuation theorem investigation of shear viscosity by molecular dynamics simulations: The information and the noise

D. M. Heyes ✉ ⓘ ; D. Dini ⓘ ; E. R. Smith ⓘ

Check for updates

View Online

Export Citation
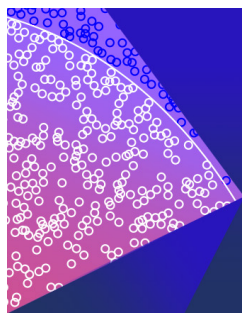
Viscuit and the fluctuation theorem investigation of shear viscosity by molecular dynamics simulations: The information and the noise

View Online   Export Citation   CrossMark

D. M. Heyes,[1,a] ⓘD   D. Dini,[1,b] ⓘD   and   E. R. Smith[2,c] ⓘD

AFFILIATIONS

[1] Department of Mechanical Engineering, Imperial College London, Exhibition Road, South Kensington, London SW7 2AZ, United Kingdom
[2] Department of Mechanical and Aerospace Engineering, Brunel University London, Uxbridge, Middlesex UB8 3PH, United Kingdom

[a] Author to whom correspondence should be addressed: d.heyes@imperial.ac.uk
[b] d.dini@imperial.ac.uk
[c] Edward.Smith@brunel.ac.uk

ABSTRACT

The shear viscosity, η, of model liquids and solids is investigated within the framework of the viscuit and Fluctuation Theorem (FT) probability distribution function (PDF) theories, following Heyes *et al.* [J. Chem. Phys. **152**, 194504 (2020)] using equilibrium molecular dynamics (MD) simulations on Lennard-Jones and Weeks–Chandler–Andersen model systems. The viscosity can be obtained in equilibrium MD simulation from the first moment of the viscuit PDF, which is shown for finite simulation lengths to give a less noisy plateau region than the Green–Kubo method. Two other formulas for the shear viscosity in terms of the viscuit and PDF analysis are also derived. A separation of the time-dependent average negative and positive viscuits extrapolated from the noise dominated region to zero time provides another route to η. The third method involves the relative number of positive and negative viscuits and their PDF standard deviations on the two sides for an equilibrium system. For the FT and finite shear rates, accurate analytic expressions for the relative number of positive to negative block average shear stresses is derived assuming a shifted Gaussian PDF, which is shown to agree well with non-equilibrium molecular dynamics simulations. A similar treatment of the positive and negative block average contributions to the viscosity is also shown to match the simulation data very well.

I. INTRODUCTION

The determination of the transport coefficients of molecular liquids has become a relatively routine and widely employed activity within the molecular simulation community. The shear viscosity, η, in particular, has been the subject of many studies because of its significance in characterizing the flow properties of liquids in numerous practical applications. The equilibrium Molecular Dynamics (MD) technique can be employed to compute the transport coefficients using the Green–Kubo (GK) equations.[1,2] The GK method involves integrating a time correlation function, $C(t)$, which quantifies the persistence in time (t) of states characterized by a certain quantity, which for η is the shear stress of the system. In recent years, there have been publications on how to most efficiently and accurately determine the plateau value of the GK time-integral, which is proportional to the viscosity.[3–9] As the simulation is of finite length in time, statistical fluctuations become an important detrimental feature whose effects increase with the correlation function time, t. In practice, in MD simulations, there is a time "window" in which the plateau needs to be extracted before the noise dominates. This problem of determining the plateau value of the GK integral is one of the themes of this work.

The decomposition of the GK-determined transport coefficients into their negative (entropy absorbing) and positive (entropy

generating) components is a recent development.[10–12] Besides providing useful insights into the physical origins of the processes that determine the value of the transport coefficient, this procedure, it will be shown, provides useful ancillary information in establishing the time at which the plateau value has been reached. In addition, a new viscuit probability distribution function based route to the shear viscosity is presented, which shows evidence of being less subject to statistical uncertainties than the original average time correlation function GK method, even though the two are formally equivalent in the thermodynamic limit.

II. VISCOSITY THEORY AND THE SHEAR STRESS AUTOCORRELATION FUNCTION

The theoretical and computational aspects of this work are considered in this section. The MD simulations are based on the Lennard-Jones (LJ) pair potential, $\phi(r) = 4\epsilon[(s/r)^{12} - (s/r)^6]$, where r is the center-to-center distance between the two molecules and ϵ and s are the characteristic intermolecular interaction energy and molecular diameter, respectively. The quantities reported in this work are given in the usual LJ reduced units, e.g., the reduced number density, $\rho^* = \rho s^3$, temperature, $T^* = k_B T/\epsilon$ (k_B is Boltzmann's constant), potential energy as $U^* = U/\epsilon$, and the same units for total energy and kinetic energy. The shear stress and pressure are given in the reduced units, $P^* = P/\epsilon s^{-3}$, time t is in, $t/sm^{1/2}\epsilon^{-1/2}$, and the reduced shear viscosity is $\eta^* = \eta/s^{-2}\epsilon^{1/2}m^{1/2}$. For compactness of notation, the asterisk superscript is omitted in the rest of this work.

A. Green-Kubo Newtonian shear viscosity

The Newtonian shear viscosity is calculated using the GK method, which employs the off-diagonal elements of the pressure tensor, e.g., P_{xy}. For the monatomic LJ fluid, the instantaneous value of P_{xy} is given by

$$P_{xy} = \frac{1}{V}\left(\sum_{i=1}^{N}\left[m_i v_{xi} v_{yi} - \frac{1}{2}\sum_{j\neq i}^{N} r_{x,ij}\frac{r_{y,ij}}{r_{ij}}\phi'(r_{ij})\right]\right), \quad (1)$$

where N is the number of molecules in volume V (typically the volume of the MD simulation cell), $v_{\alpha i}$ is the α component of the velocity of the molecule i or $\underline{v}_i$, and $r_{\alpha,ij}$ is the α component of the pair separation vector between molecules i and j. The first derivative of $\phi(r)$ is denoted by ϕ'. The shear stress autocorrelation function, $C_s(t)$, and its relation to the shear viscosity and derived quantities are

$$C_s(t) = \langle P_{xy}(0)P_{xy}(t)\rangle, \quad \eta(t) = \frac{V}{k_B T}\int_0^t C_s(t')dt',$$

$$\eta = \lim_{t\to\infty}\eta(t), \quad G_\infty = (V/k_B T)\langle P_{xy}^2\rangle, \quad C(t) = C_s(t)/C_s(0), \quad (2)$$

$$\tau_s = \int_0^\infty C(t')\,dt', \quad \eta = G_\infty\tau_s,$$

where $C(t)$ is the same function normalized by its $t = 0$ value, which is the standard way of plotting the shear stress autocorrelation function in this work. The formalism $\langle\cdots\rangle$ indicates an average over time origins (i.e., time in the simulation declared to be $t' = 0$) and subsequent times over a simulation. The time dependent viscosity is denoted by $\eta(t)$, and its long time limit is the shear viscosity (i.e., without the "t" argument). The "instantaneous" or infinite fre-

quency shear rigidity modulus is denoted by G_∞ in Eq. (2), and τ_s is the shear stress relaxation or "Maxwell" time.[13] The product $G_\infty\tau_s$ is Maxwell's expression for the shear viscosity, which forms the basis of this formulation of viscoelasticity. The time correlation function, $C_s(t)$, is the shear stress relaxation function in the limit of the zero shear rate encountered in the subject of rheology. For simplicity of notation, the shear stress, $\sigma = -P_{xy}$, is used below.

$C(t)$ and $\eta(t)$ are prone to significant statistical uncertainties in practice because the shear stress is a whole system property, and therefore, only one value of σ for each off-diagonal element of the stress tensor is obtained each time step. From a practical point of view, η is obtained by establishing the plateau value of $\eta(t)$ at long times. This is hampered by the development of statistical fluctuations in $C(t)$ and hence $\eta(t)$ typically in more or less the same time region where the plateau in $\eta(t)$ is starting to form. Its effects can be mitigated to some extent by carrying out longer simulations, at least for small molecules, but for large flexible molecules where the stress relaxation processes are slower and the computational demands higher, it becomes more problematic to achieve this separation of signal and noise time scales. Previous theory and simulations[3–5] reveal that the standard deviation in the correlation function and its time integral at long times scales as $\sim(\tau/T_{sim})^{1/2}$, where τ is a characteristic relaxation time of the correlation function and T_{sim} is the total simulation time.

The plateau in $\eta(t)$ can be obtained by fitting $C(t)$ to an expression and then integrating this analytically to determine $\eta(t)$. Hartkamp et al. used a fit to $C(t)$, which was the sum of a Gaussian and two exponentials (the Gaussian dominates in the "ballistic" regime at short time).[14] An alternative formula, a sech and two exponentials, was proposed in Ref. 10, which was found to match better the molecular dynamics correlation function data considered in that study. The analytic expression of the sech function $C_s(t)$ is

$$C_s(t) = G_\infty\big(A\,\text{sech}(t/\tau_1) + B\,\exp(-t/\tau_2)$$
$$+ (1 - A - B)\exp(-t/\tau_3)\big),$$

$$\eta(t) = G_\infty\big(A\tau_1\,\tan^{-1}[\sinh(t/\tau_1)]$$
$$+ B\,\tau_2[1 - \exp(-t/\tau_2)]\big) + G_\infty(1 - A - B)\tau_3 \quad (3)$$
$$\times[1 - \exp(-t/\tau_3)],$$

$$\eta = \lim_{t\to\infty}\eta(t) = G_\infty\left(\frac{\pi}{2}A\tau_1 + B\tau_2 + (1 - A - B)\tau_3\right).$$

The dimensionless coefficients, A and B, and the three relaxation times, τ_1, τ_2, and τ_3, can be obtained by least squares fitting the MD-determined $C_s(t)$ to the first formula in Eq. (3). The two exponentials in Eq. (3) reproduce well the long time behavior of $C_s(t)$ beyond the ballistic region. The sech term also tends to an exponential at long times.

III. VISCUITS

The shear viscosity can be recast as the first moment of a probability distribution function (PDF) of the single trajectory (ST) contributions or "viscuits." A viscuit is a single trajectory contribution to the GK viscosity average indicated in Eq. (2), which is the quantity that is used in reformulating the Green–Kubo method. This idea was proposed by Stillinger and Debenedetti[15] and shares some features in

common with Erpenbeck's "hybrid" extension of GK.[16] The definition of the viscuit, $\eta_u(t)$, and its relationship to the time-dependent viscosity, $\eta(t)$, is

$$\eta_u(t) = \frac{V}{k_B T} \int_0^t \sigma(0)\sigma(t')dt',$$

$$\eta(t) = \langle \eta_u(t) \rangle$$

$$= \int_{-\infty}^{\infty} d\eta_u(t)\, \eta_u(t)\, P(\eta_u(t)). \quad (4)$$

The viscuit defined in the first line of Eq. (4) is just one contribution from a specific trajectory to the GK integral, which is already available in the standard GK MD treatment but whose statistics are not normally investigated.[17] Formally, $\eta_u(t)$ involves an integral up to time t and is defined starting from the stress at a single specific time ("time origin") during the simulation. In a simulation, the first integral in Eq. (4) is replaced by a summation of the instantaneous stress evaluated at time intervals of the simulation time step. The PDF $P(\eta_u(t))$ is the probability distribution function of $\eta_u(t)$. In the second line of the above equation, $\eta(t)$ is written as the average of the viscuits. The viscuit at any given time can be negative or positive, and these can be averaged separately during the simulation. In the final line of Eq. (4), the time dependent viscosity is written as the first moment of the PDF of the viscuits evaluated up to a predefined value of t. There is a different PDF for each value of t, but the PDF is found to converge to a limiting form for large t, i.e., of several Maxwell relaxation times. For typical LJ liquid states, this is typically in the time range $t = 2$–3 reduced units, depending on the temperature and density.

A. Simulation details

The state point mainly used here was $\rho = 0.8442$ and $T = 0.722$, which is referred to as "R1," which is close to the triple point of the LJ system and has become a standard or reference liquid state point for this generic molecular liquid (see Refs. 2, 18, and 19 for their original use, and there is a more recent compendium of triple point density and temperature values in Ref. 20). A table of literature values of the shear viscosity at the LJ R1 state point is given in Ref. 21, and a series of η values for different N is presented in Ref. 22. The R1 state point shows the highest liquid state viscosity and has the most persistent structure in the long time region of the stress relaxation function (i.e., more pronounced viscoelastic behavior), which is characteristic of more structured liquids composed of small polyatomic molecules. With increasing temperature and decreasing density, the LJ viscosity decreases and the time correlation function decays more rapidly and becomes more featureless (characteristic of a dense supercritical fluid than a typical liquid). We note that the chosen state point is close to the two-phase vapor–liquid boundary, and care is required to ensure that the simulations are in the one-phase region.

Simulations were also conducted at the same density and temperature using the Weeks–Chandler–Andersen (WCA) potential,[23] which is the repulsive part of the LJ potential. This density and temperature are also in the dense fluid part of the WCA phase diagram.[24] A comparison of results computed at this density and temperature for the two potentials helps to discern the effects of the attractive part of a potential on the computed properties. This comparison also helps to identify those properties that depend on the details of the

potential and those that do not. Some simulations were carried out for solid state points to assess further the range of applicability of the viscuit theory. The temperature was controlled by the Nosé–Hoover thermostat,[25] with a time constant of 3 LJ time units.

In regard to the fluctuation theorem, other simulations were carried out at the finite shear rate using the SLLOD equations of motion to implement planar Couette flow.[26,27] This is an example of a Non-equilibrium Molecular Dynamics (NEMD) simulation. The calculated quantities are given in units of ϵ and σ and the mass of the molecule, m. Quantities denoted with a "LJ" subscript indicate that they are given in these units and can apply therefore to simulations carried out with the LJ or WCA potentials. The interaction cutoff was 2.5, and the simulations were carried out for between 10^5 and 2×10^7 time steps.

B. Negative and positive contribution to the viscuit

Figure 1(a) shows the normalized shear stress correlation function, $C(t)$, of a liquid LJ state near the triple point split into its negative and positive components, $C_-(t)$ and $C_+(t)$ (i.e., those that come from a negative or positive viscuit at time t, respectively). A fit to the total correlation function using the sech formula in Eq. (3) is also shown. The positive component is more slowly decaying than the total function, and the negative component decreases from 0 at $t = 0$. At short times, $C(t)$ is determined mainly by $C_+(t)$, as the product of two quantities at two closely separated times must be predominantly positive because the two states are strongly correlated. With an increase in time, the contribution $C_-(t)$ increases from zero, and this development is, in fact, responsible for the rapid decay of the total correlation function, $C(t)$, to zero at long times. $C_-(t)$ and $C_+(t)$ individually are slow to decay on the same time scale, but their effects cancel out at long times and the total correlation function decays more rapidly to zero.

Figure 1(a) also shows $-C_-(t)$, which is seen to be statistically indistinguishable from $C_+(t)$ for times in excess of $\simeq 1.5$. The long time decay of the two components scales as $t^{-1/2}$ but with opposite prefactor signs. Figure 1(b) shows the corresponding plot for the WCA potential carried out at the same density and temperature (i.e., $\rho = 0.8442$ and $T = 0.722$) and exhibits the same trends as the LJ system. The $\sim t^{-1/2}$ scaling of the correlation function components arises from random fluctuations in the product of two stresses widely separated in time. The reason for this particular exponent value becomes clearer in Fig. 2 and its associated discussion.

The time dependent viscosity, $\eta(t)$, defined in Eq. (2) applied to the data in Fig. 1 is shown in Fig. 2(a), together with the same quantity derived from the analytic sech fit formula given in Eq. (3). The total $\eta(t)$ of the WCA fluid in the large t limit is about two-thirds of the LJ value presumably because the LJ liquid is a more cohesively held together fluid than the WCA case, whose potential is purely repulsive. The average of the positive and negative viscuit components is also presented in Fig. 2(a). Figure 2(b) shows the same data plotted as a function of $t^{1/2}$. A least squares fit to the limiting region of $\eta_-(t)$ and $\eta_+(t)$ also shown in this figure reveals that $\eta(t)$ increases as $t^{1/2}$ at times longer than several Maxwell relaxation times. It takes the negative contribution longer to achieve the $t^{1/2}$ scaling region than the positive contribution. This long time scaling can be rationalized on the basis of the known statistics of $\eta(t)$, whose exact expressions are
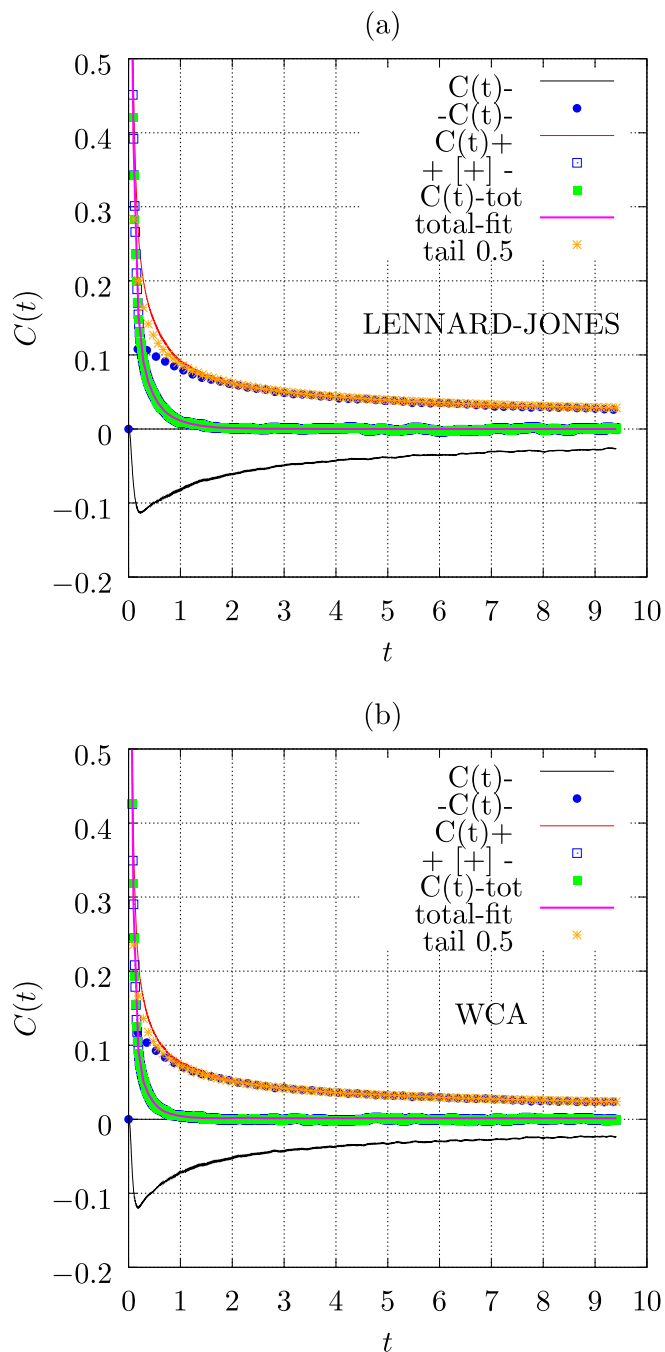
FIG. 1. (a) Normalized shear stress correlation function, $C(t)$, used in the GK method for the shear viscosity, which is also fitted to the sech formula in Eq. (3) ("total-fit"). The contributions from the negative and positive viscuits, $C_-(t)$ and $C_+(t)$, respectively, are shown. The sech fit formula parameters are $A = 0.7415$, $B = 0.1745$, $\tau_1 = 0.049\,1(1)$, $\tau_2 = 0.1982$, and $\tau_3 = 0.4698$. The figure also shows the same data except that $-C_-(t)$ is plotted, and a fit of the form $A/t^{1/2}$ to $C_+(t)$ is given in the figure. The Lennard-Jones potential was used, with the other parameters $\rho = 0.8442$ and $T = 0.722$, $N = 256$ particles, and 10^7 time steps. (b) The same plot for the WCA fluid with otherwise the same input parameters. The sech formula fit parameters are $A = 0.8408$, $B = 0.1576$, $\tau_1 = 0.042\,89$, $\tau_2 = 0.2400$, and $\tau_3 = 74.7$.
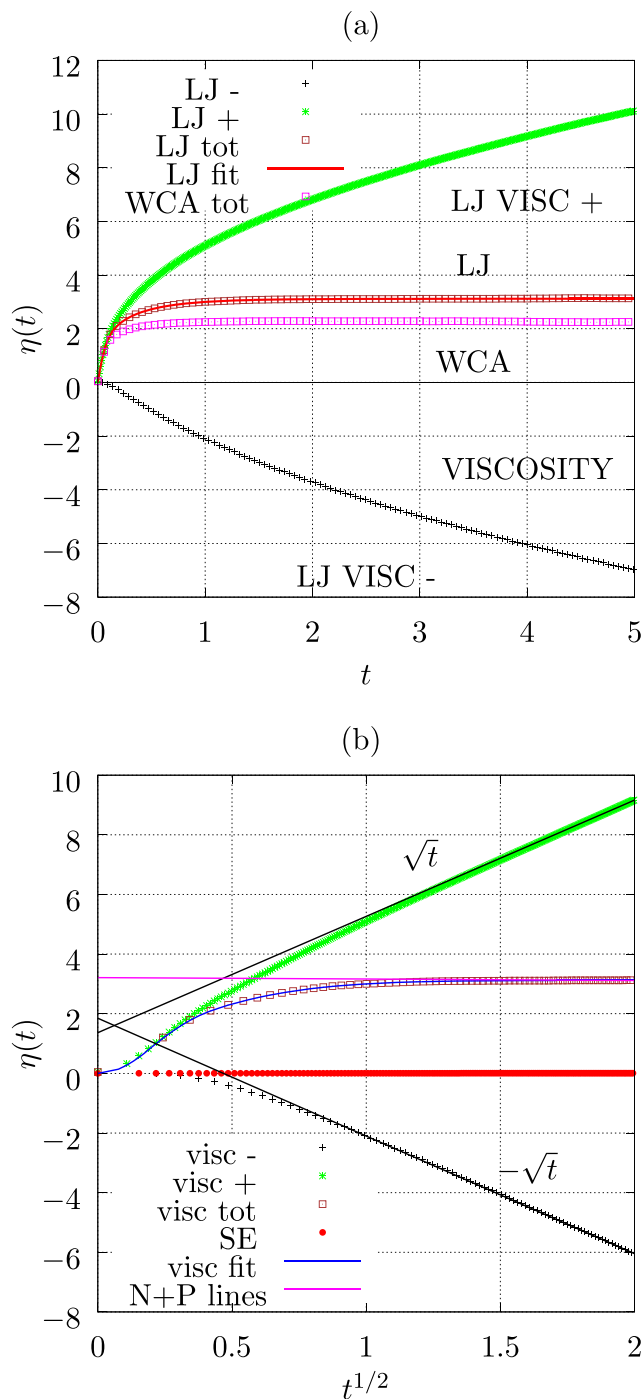
FIG. 2. (a) The time dependent LJ viscosity, $\eta(t)$, using the data from Figs. 1 and 2. The analytic sech fit formula from Eq. (3) is shown, as are the average of the positive and negative viscuits, shown separately. (b) Same as (a) except the data are plotted as a function of $t^{1/2}$. This shows that $\eta_-(t)$ and $\eta_+(t)$ scale as $t^{1/2}$ at long times. The fit parameters to the equations in Eq. (6) are $a_- = 1.85(1)$, $b_- = 3.95(2)$, $a_+ = 1.36(1)$, and $b_+ = 3.90(2)$, and therefore, $\eta = a_- + a_+ = 3.21(1)$. The $t^{\pm 1/2}$ scaling seen in Figs. 1 and 2 is indicative of the "noise" region in the data at long times.

$$\eta(t) = \eta_-(t) + \eta_+(t),$$

$$\eta_{u,-}(t) = \frac{V}{k_B T} \int_0^t \sigma(0)\sigma(t')dt' \quad < 0, \quad \eta_-(t) = \langle \eta_{u,-}(t) \rangle_-,$$

$$\eta_{u,+}(t) = \frac{V}{k_B T} \int_0^t \sigma(0)\sigma(t')dt' \quad > 0, \quad \eta_+(t) = \langle \eta_{u,+}(t) \rangle_+,$$

$$\eta_u(t) = \frac{V}{k_B T} \int_0^t \sigma(0)\sigma(t')dt', \quad \eta(t) = \langle \eta_u(t) \rangle,$$

$$P(\eta_u(t)) = P(\eta_{u,-}(t)) + P(\eta_{u,+}(t)),$$

$$P(\eta_{u,-}(t \to \infty)) = P(\eta_{u,+}(t \to \infty)),$$

$$(5)$$

where $P(x)$ is the probability of x and the notation $\langle \cdots \rangle_\pm$ indicates an average of the viscuits for time, t, whose magnitudes have either the − or + sign. The equality in the two sub-PDFs at long times given in the last line of Eq. (5) is because the short time "correlated" region should contribute a progressively smaller proportion to the total in the large t (or noise-dominated) limit. The long time form of the contributions to the viscosity integral from the two sides is established using Gaussian statistics. In the long time limit, the viscuit standard deviation in the total time dependent viscosity, $\eta(t)$, follows a $t^{1/2}$ scaling.[5,28] For a half-normal distribution, the mean and standard deviation are proportional to each other and also to the standard deviation of the combined PDF valid over the whole viscuit domain.[29] Therefore, the $\eta_-(t)$ and $\eta_+(t)$ individually should also scale as $t^{1/2}$, assuming Gaussian statistics. Hence, the difference between $\eta_-(t)$ and $\eta_+(t)$ for large t is also a measure of the breadth of the $\eta(t)$ distribution of each side in the large t limit.

The limiting dependence of $\eta(t)$ on time is consistent (by differentiation) with $C_-(t)$ and $C_+(t)$ decaying as $t^{-1/2}$. Figure 1(a) demonstrates that the MD data follow this dependence. To summarize, Figs. 1 and 2 show that the correlation function can be separated into two limiting regions in the small and large time limits, between which the stress correlation between consecutive time steps dominates, where at long times, the noise is the important factor. Although in the LJ fluid, the repulsive and attractive parts of the potential give positive and negative contributions to the viscosity, the quantities η_- and η_+ defined here are different quantities and are present even for purely repulsive potentials [i.e., WCA, see Fig. 1(b)]. In fact, there *always* has to be a $\eta_-(t)$ contribution to the time-dependent viscosity for any molecular system; otherwise, $\eta(t)$ would not converge to a plateau value. The statistics of $\eta_-(t)$ and $\eta_+(t)$ are rigorously determined by Gaussian statistics in the large t limit.

The large t time dependence of $\eta_-(t)$ and $\eta_+(t)$ leads to a direct route to η. In the $t \to \infty$ limit, where the slopes in a $\sqrt{t}$ plot of the two viscuit sides will be equal in magnitude and opposite in sign,

$$\eta_-(t) = a_- - b\sqrt{t}, \quad \eta_+(t) = a_+ + b\sqrt{t},$$

$$\eta_-(t \to \infty) + \eta_+(t \to \infty) \equiv \eta = a_- + a_+,$$

$$(6)$$

$$\frac{\eta_-(t \to \infty)}{\eta_+(t \to \infty)} = -1.$$

The sum of the intercepts, $a_- + a_+$, is 3.21(1) for the LJ fluid, which is in very good agreement with the value obtained by GK and other PDF routes discussed below. The slopes of the negative and positive components achieve a limiting value of ±3.9 for times greater

than ~1.7 time units, which is statistically the same as noted above. In the limit of $t \to \infty$, the noise dominates, and in practice, information about the viscosity is lost and the ratio of the two contributions tends to −1. On the time scale of a simulation, however, the $\sqrt{t}$ dependence of the viscosity components provides another route to η and its negative and positive components. The noise, which is usually considered to be an unwanted feature of GK calculations in the plateau region, can therefore be exploited via Eq. (5) to compute the viscosity. The simulation data used for Figs. 1 and 2 are given in the supplementary material. In addition, the procedure used to generate Fig. 2 was repeated for the LJ state point $\rho = 0.8$ and 1.0 (or "R2") and presented in Fig. 2 of the supplementary material. This state point is near the middle of the LJ liquid domain. The value of the Lennard-Jones viscosity obtained from Eq. (6) for R2 is 2.09(1), which is the same as that using standard GK reported in Table I of Ref. 11.

Crystals exhibit viscoelastic properties and a limiting shear viscosity, which is only a little higher than that of a coexisting liquid, at least for a simple system such as the WCA or LJ.[30] Figure 3 shows $\eta_-(t)$ and $\eta_+(t)$ and total viscosity for a LJ solid. This figure also demonstrates that the $t^{1/2}$ scaling is clearly evident for $\eta_+(t)$ but takes a little longer to become established in $\eta_-(t)$ in the solid.

To summarize, the statistical fluctuations, which, in practice, give rise to uncertainties in the plateau value of the integrated time correlation function in the GK method, do have a practical use. By extrapolation of the data from the noise-dominated region to zero time, the contributions to the viscosity from the negative and positive parts of the viscuit PDF can be assigned at any time, and the total viscosity is simply determined by adding the two intercepts [see Eq. (6)]. Figure 3(b) shows the ratio $\eta_-(t)/\eta_+(t)$ as a function of time for the LJ and WCA fluids at the reference state point. This quantity is monotonically varying with time and approaches the −1 limit for $t \to \infty$ quite slowly. A comparison with Fig. 2(b) shows that the $t \to \infty$ limit is best incorporated in any treatment by taking the local slope of the negative and positive side curves.

C. PDF definitions and viscosity formulas

There are a number of ways of computing the shear viscosity from the viscuit PDFs, depending on how the viscuit PDF is defined.

1. PDF defined over the whole domain

The PDF, $P(\eta_u(t))$, given in Eq. (4) corresponds to the case where the viscuit is in real units (i.e., here LJ) and where $-\infty < \eta_u(t) < \infty$. The integral of the PDF over this complete argument range is set to unity by a normalization constant. The $\eta_u(t)$ quantity is represented for conciseness in the following equations by "x," which, note, has an implicit time or "t" dependence. The PDF in $P(x)$ is not symmetric on the negative and positive sides,[11,12] and the difference between the two leads directly to a definition of the simulation average quantity, $\eta(t)$ (and hence the viscosity itself by taking the $t \to \infty$ limit),

$$\eta(t) = \eta_+(t) + \eta_-(t)$$

$$= \int_{-\infty}^0 x P(x)\, dx + \int_0^\infty x P(x)\, dx$$

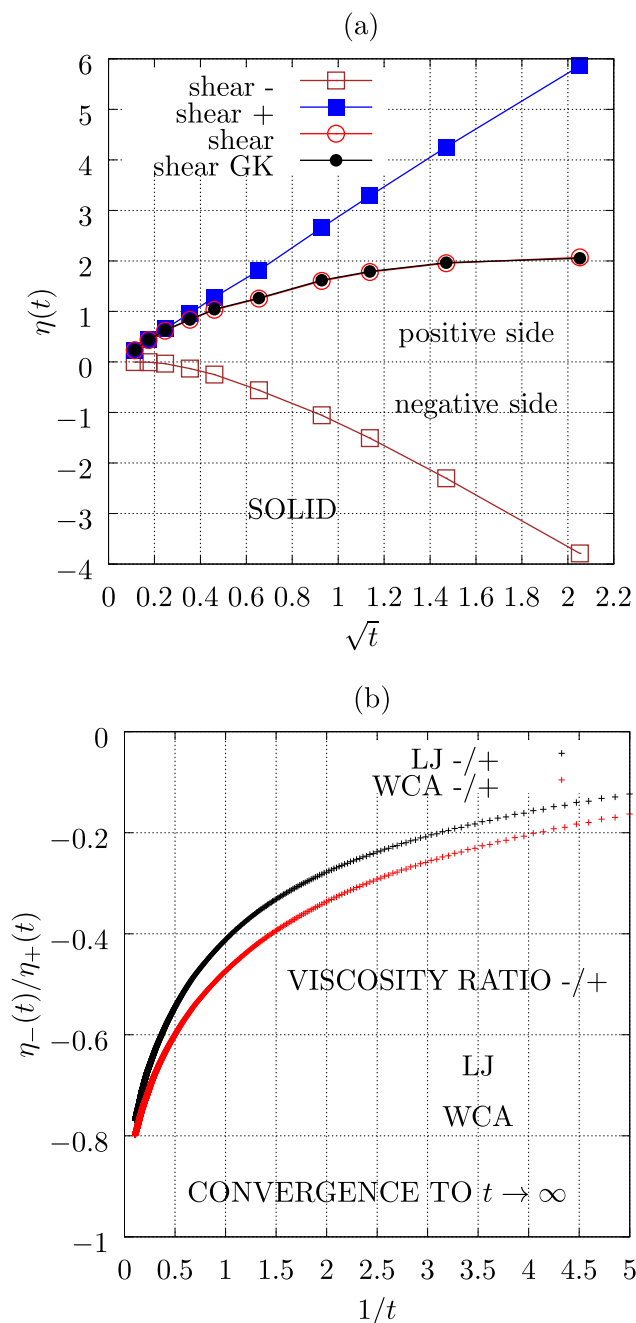$$= \int_0^\infty x[P(x) - P(-x)]\, dx. \quad (7)$$

FIG. 3. (a) The time dependent shear viscosity, η, as a function of $\sqrt{t}$ for a LJ solid state point where $\rho = 1.1$ and $T = 0.80$. The MD data for the viscuit first moment of the PDF are compared with the GK time correlation formula. The formulas for both approaches are given in Eq. (4). (b) The ratio η_-/η_+ from Eq. (5) as a function of t^{-1} for the LJ and WCA fluids at the same density and temperature, $\rho = 0.8442$ and $T = 0.722$. The long time limit of the ratio is -1.

The potential advantage of this route is that the subtraction in Eq. (7) may cancel out, at least partially, the fluctuation or "noise" derived contributions to the PDF, which is unavoidable in practical GK MD calculations [and is manifest in the $\sqrt{t}$ dependence of the

component viscuit averages shown in Fig. 2(b)]. These contributions will be present at *all t*, not just in the large "$\sqrt{t}$" limit.

Figure 4(a) compares the $\eta(t)$ obtained by GK from Eq. (2) and the PDF route of Eq. (7). On the left-hand side of the plot are the
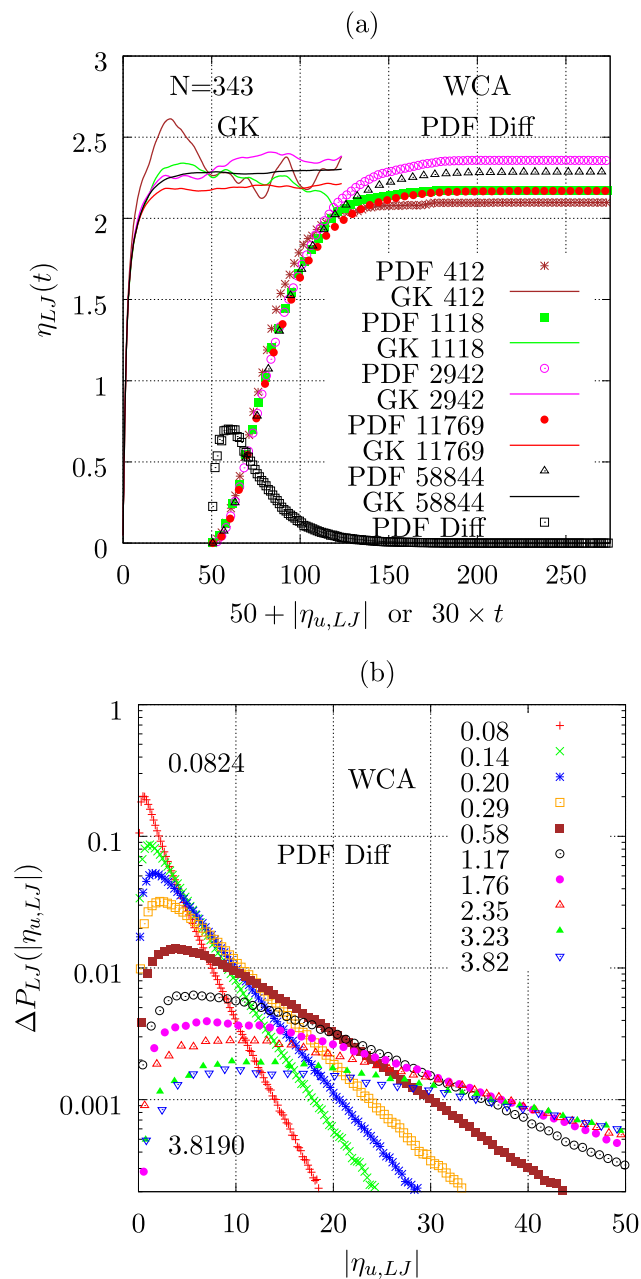

FIG. 4. (a) The time-dependent viscosity from GK (time scaled by ×30) and the single PDF difference formula of Eq. (7) plotted as a function of the viscuit value for $t = 2.35$ and for different simulation times, t_{sim}, which are given in the figure. The WCA potential was used at the reference state point, $\rho = 0.8442$ and $T = 0.722$, with $N = 343$. The difference in the parts of the single WCA PDF on the two sides, $\Delta P_{LJ}(|\eta_{u,LJ}|)$, are also shown (magnified by a factor of ×250). (b) Same as for (a) except the $\Delta P_{LJ}(|\eta_{u,LJ}|)$ for the corresponding WCA state point are given (without magnification) for different t values, which are indicated in the figure.

GK time dependent viscosities, $\eta(t)$, obtained by integration of the time correlation function and given as continuous curves. On the right-hand side of this figure are the corresponding PDF viscosities as a function of the viscuit value, shown as symbols. The various colored curves and symbols are for different total simulation times, which are indicated in Fig. 4(b). Both show a plateau range when the argument (i.e., explicit time or absolute viscuit) magnitude is large. The difference between the positive and negative sides of the PDF, $\Delta P_{LJ}(x) = [P(x) - P(-x)]$, for the longest simulation time case is also shown magnified at the bottom of Fig. 4(a). It shows a rapidly rising ascent followed by a monotonically decaying tail. Data for the WCA fluid are presented.

Although formally equivalent, upon sufficient averaging, the PDF method exhibits smaller fluctuations than the GK method for large arguments and for the same simulation length and other parameters. For example, for the longest total simulation length (58 844 reduced time units), the GK and PDF WCA shear viscosities are 2.29(1) and 2.286(3), with the uncertainties in the last digit in brackets. The corresponding LJ simulations give 3.10(3) and 3.144(3). This indicates that the PDF route has a lower statistical uncertainty than the GK route. The difference in the statistical uncertainty, in fact, shows up in a more pronounced way for short simulation lengths. Even for quite short run,s the PDF route exhibits a well-defined plateau, but the GK "plateau" is extremely noisy, as may be seen in Fig. 4(a). A partial cancellation of the noise in the negative and positive sides of the PDF in the expression in Eq. (7) may be the reason for this difference in behavior. In addition, the PDF approach to the viscosity generally may be intrinsically better formulated to "filter" out the noise. The qualitative difference between the GK and viscuit routes results from differences in the form of the integrand in the two cases. The stress autocorrelation function has a slowly decaying tail in the noise-dominated time range, while the PDF differences decay more rapidly at high values of the stress, which gives rise to a more smoothly converging integral.

However, it should be noted that the value of the PDF plateau *does* vary with simulation time, following generally the long-time average of the GK integral (although this region can be seen to be more noisy in the GK case). Therefore, the optimum simulation lengths will be similar irrespective of whether GK or this PDF route is used, but the PDF method does always gives a better defined plateau than the GK route for any given simulation length. These preliminary results indicate that the viscosity can be defined more precisely by the PDF method. A more extended study would be required, however, for example, on the relative rates of convergence with argument upper limit, before it could be established whether the PDF route has practical advantages over the usual GK approach in determining the viscosity.

Figure 4(b) presents $\Delta P_{LJ}(|\eta_{u,LJ}|)$ on a lin–log scale for a range of t values at the reference state point using the WCA potential. As t increases, the quantity broadens out, and its peak shifts to higher values of $\eta_{u,LJ}$. They all show an exponential decay in the large viscuit limit. Data for another LJ and WCA state point, R2, where $\rho = 0.8$ and $T = 1.0$, which is near the middle of the LJ liquid range, are presented in supplementary material. The figures corresponding to Figs. 1, 2, 4, and 5 are also shown, which demonstrates that the trends are the same and therefore not unique to any particular liquid state point.
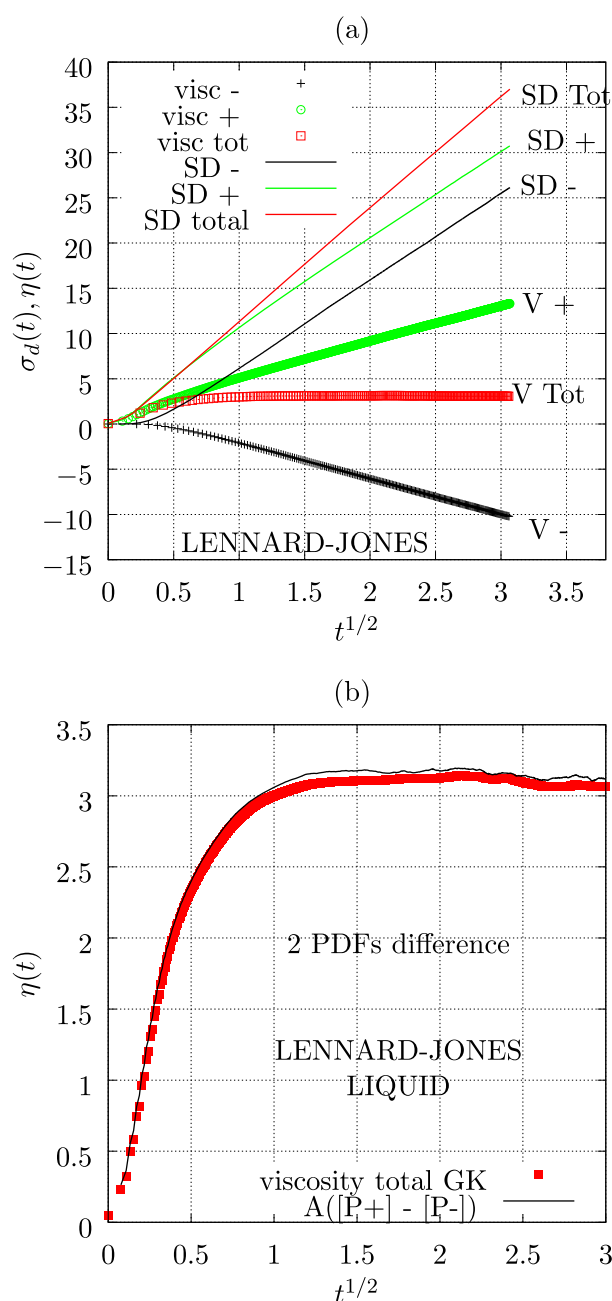

FIG. 5. (a) The $\eta_-(t)$ and $\eta_+(t)$ and the time dependent standard deviation (SD) of the corresponding viscuits. (b) compares the time-dependent viscosity obtained by GK and that obtained by the PDF route of Eq. (10). The A constant formula in Eq. (10) was assigned the value $A = 0.817$ obtained by least squares fit to the MD P_0 data. The LJ potential was used for the $\rho = 0.8442$ and $T = 0.722$ state point, where $N = 256$ particles and there were 10^7 time steps.

The distribution of viscuits for a given t can be characterized to low order by its standard deviation $\sigma_d(t) = [\langle \eta_u(t)^2 \rangle - \langle \eta_u(t) \rangle^2]^{1/2}$. The standard deviation of the viscuit plays a central role in defining different possible PDFs and the relationships between them.

2. PDF defined separately on the two sides

As $P(x)$ is not symmetric between the negative and positive sides,[11,12] one alternative and appropriate representation is to define two distinct PDFs: one is $P_-(x)$ for the negative argument range $-\infty < x < 0$, and the other is $P_+(x)$ for $0 < x < \infty$. Each one-sided PDF is normalized separately so that the integrals on both sides are each equal to 1. The standard deviation of the two PDFs, $\sigma_{d,-}$ and $\sigma_{d,+}$, respectively, are given by

$$
\begin{aligned}
\sigma_{d,-}^2 &= \int_{-\infty}^{0} x^2 P_-(x)\,dx - \left[\int_{-\infty}^{0} x P_-(x)\,dx\right]^2, \\
\sigma_{d,+}^2 &= \int_{0}^{\infty} x^2 P_+(x)\,dx - \left[\int_{0}^{\infty} x P_+(x)\,dx\right]^2,
\end{aligned}
\tag{8}
$$

respectively.

It was also found in Ref. 11 that if x is defined as the viscuit divided by its standard deviation (treated separately for each side), then the two PDFs are statistically indistinguishable for not too small t. These scaled-argument PDFs are defined by a single function, $P_{0,\pm}$, which are related to their unscaled versions as follows:

$$
P_{0,-}\left(\frac{x}{\sigma_{d,-}}\right) \quad -\infty < x < 0, \quad P_{0,+}\left(\frac{x}{\sigma_{d,+}}\right) \quad 0 < x < \infty,
$$

$$
\int_{-\infty}^{0} P_-(x)\,dx = 1, \quad \int_{0}^{\infty} P_+(x)\,dx = 1,
$$

$$
\int_{-\infty}^{0} P_{0,-}\left(\frac{x}{\sigma_{d,-}}\right)\frac{dx}{\sigma_{d,-}} = 1, \quad \int_{0}^{\infty} P_{0,+}\left(\frac{x}{\sigma_{d,+}}\right)\frac{dx}{\sigma_{d,+}} = 1,
$$

$$
P_{0,-}\left(\frac{x}{\sigma_{d,-}}\right) = \sigma_{d,-} P_-(x), \quad P_{0,+}\left(\frac{x}{\sigma_{d,+}}\right) = \sigma_{d,+} P_+(x),
\tag{9}
$$

where the relationships on the last line of Eq. (9) follow directly from the definitions on the second and third lines. It was found in Ref. 11 that $P_{0,-}(-X/\sigma_{d,-}) = P_{0,+}(X/\sigma_{d,+}) \equiv P_0(y)$ for $X > 0$ and $y = -X/\sigma_{d,-}$ or $X/\sigma_{d,+}$, where appropriate. The non-dimensionalized argument PDFs $P_{0,-}$ and $P_{0,+}$ are therefore observed in the large t limit to be symmetric on the negative and positive argument sides. This can be exploited in another definition of the time-dependent viscosity as follows.

Equation (4) combined with the relations in the last line of Eq. (9) gives a simple expression for the time dependent viscosity, $\eta(t)$, in terms of the standard deviations of the two (real unit) PDFs. The quantity, $\sigma_{d,\pm}$, has units of viscosity, and the dimensionless variable, $y = x/\sigma_{d,\pm}$, is used below. One of the features of treating the two halves of the PDF separately is that an additional piece of information about the two sides is required to make further theoretical progress, which is the relative number of occurrences of the negative and positive viscuits. Let $R_- = N_-/[N_- + N_+]$ and $R_+ = N_+/[N_- + N_+]$, where N_- and N_+ are the number of occurrences of negative and positive viscuits, respectively, during the simulation. Then,

$$
\begin{aligned}
\eta(t) &= \eta_-(t) + \eta_+(t) \\
&= R_- \int_{-\infty}^{0} x P_-(x)\,dx + R_+ \int_{0}^{\infty} x P_+(x)\,dx \\
&= \sigma_{d,-}^2 R_- \int_{-\infty}^{0} y \frac{P_{0,-}(y)}{\sigma_{d,-}}\,dy + \sigma_{d,+}^2 R_+ \int_{0}^{\infty} y \frac{P_{0,+}(y)}{\sigma_{d,+}}\,dy \\
&= \sigma_{d,-} R_- \int_{-\infty}^{0} y P_{0,-}(y)\,dy + \sigma_{d,+} R_+ \int_{0}^{\infty} y P_{0,+}(y)\,dy,
\end{aligned}
$$

$$
\eta(t) = A(\sigma_{d,+} R_+ - \sigma_{d,-} R_-), \quad A = \int_{0}^{\infty} y P_0(y)\,dy > 0, \tag{10}
$$

$$
\frac{\eta_-(t)}{\eta_+(t)} = -\frac{\sigma_{d,-} R_-}{\sigma_{d,+} R_+}, \quad \left|\frac{\sigma_{d,-} R_-}{\sigma_{d,+} R_+}\right| < 1,
$$

where A is dimensionless. Note that in Eq. (10), x is the viscuit and y is the viscuit scaled by the standard deviation of x for one of the sides. In addition, note that x and y have an implicit integral of the viscuit up to a time t in their definition. The penultimate line in Eq. (10) gives another definition of $\eta(t)$, which requires a value of A. Numerical integration of the simulation-derived P_0 from a specific simulation gave the value $A = 0.817(2)$. The condition in the last line of Eq. (10) holds because $\eta(t)$ must be positive to satisfy the condition that the heat production rate (which is proportional to the viscosity) is, on average, positive during shearing.

Figure 5(a) shows the viscuit standard deviation of the $\eta_{u,-}(t)$, $\eta_{u,+}(t)$, and $\eta_u(t)$. These are plotted against $t^{1/2}$ together with the corresponding $\langle\eta_{u,-}(t)\rangle$, $\langle\eta_{u,+}(t)\rangle$ and $\langle\eta_u(t)\rangle$. In general, the standard deviations increase more rapidly with time than the average viscosity itself. The total viscuit standard deviation is larger than that of the two components, whereas the total viscosity is in between the negative and positive contributions.

Figure 5(b) compares the GK formula for the time dependent shear viscosity and that obtained from the formula in Eq. (10), which involves the two standard deviations and the relative number of negative and positive viscuit occurrences. The PDF route agrees well with the GK in the ascending region and gives a plateau value, which is close to the GK value and probably within the mutual uncertainties of the two approaches, especially as A itself has some statistical uncertainty. The formula for the time dependent viscosity in the penultimate line of Eq. (10) is therefore validated.

Figure 6(a) shows the ratio $N_-(t)/N_+(t)$ as a function of $\sigma_{d,-}/\sigma_{d,+}$ for the LJ and WCA reference state point. These are statistically indistinguishable over the accessible range, and the curve is concave. At short times, the relative probability of there being negative viscuits tends to zero more rapidly than the standard deviation ratio, as evident in the curvature. In the large t limit [from left to right on Fig. 6(a)], both (absolute) ratios tend to unity. At long times, the viscuit will tend in effect to be the sum of random numbers whose statistics is the same for negative and positive sides. Any correlation effects at short time in the averaging become numerically insignificant in this long time limit (top right hand corner). The trend in the data represents a transition to zero contribution from the negative side as $t \to 0$ [bottom left of Fig. 6(a)] to purely random statistics (top right) as $t \to \infty$.

Figure 6(b) presents the ratio $-[\eta_-(t)/\eta_+(t)]$ as a function of $\sigma_{d,-}/\sigma_{d,+}$, which is seen now to be a convex function (again for data
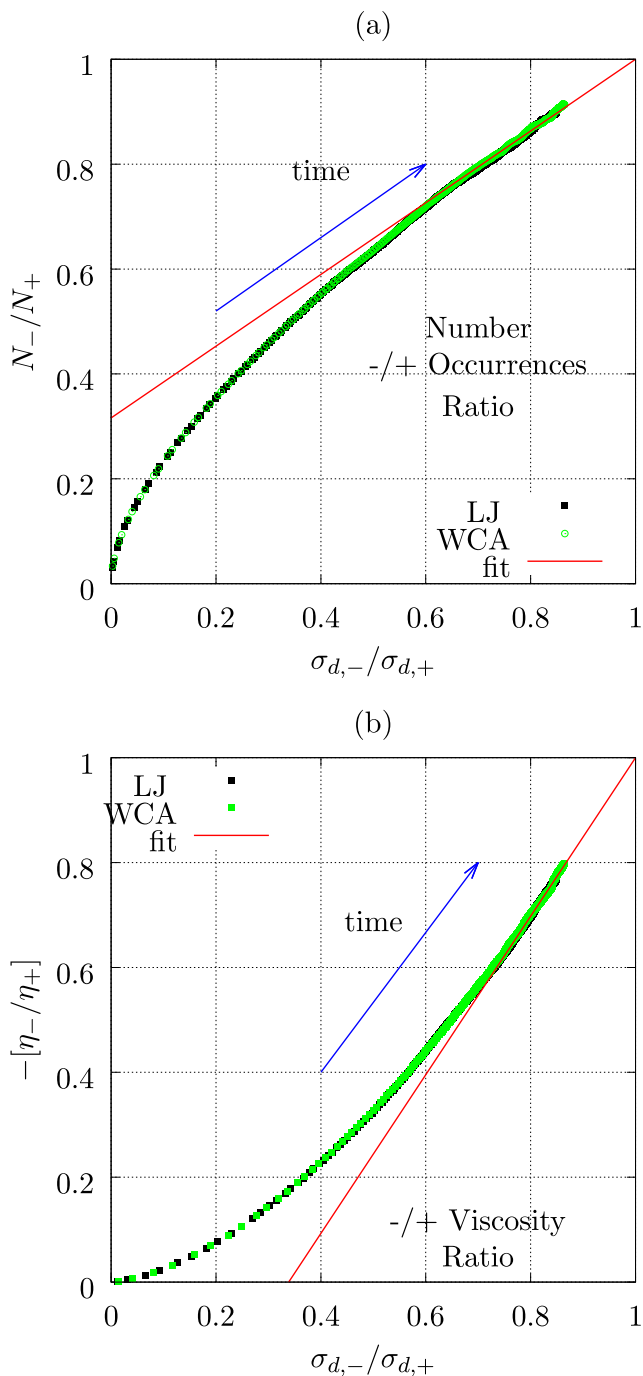
FIG. 6. (a) The ratio of the number of negative to positive viscuit occurrences against the corresponding standard deviation ratio. The linear regression slope and intercept of the large t fit (red line) are 0.683 8(4) and 0.316 2(4), respectively. (b) The ratio of the negative to positive viscosity contributions against the corresponding standard deviation ratio. The slope and intercept are 1.511 7(3) and -0.511 7(3), respectively. The red lines in (a) and (b) are linear regression fits to the data in the large t limit, constrained to having the exact $t \to \infty$ limits. The points are the MD data at the same LJ and WCA state points as for Figs. 1 and 2. Note that time t increases from left to right on the figure.

where time increases from left to right). The viscosity ratio converges more slowly to zero than the standard deviations ratio at short times, evident from the curvature in that region. At long times, these two ratios tend to unity, whereas at short times, the ratio tends to zero. These are the same limits as evident in Fig. 6(a) for the number ratios. The shape of the ratio plots in Figs. 6(a) and 6(b) is different, however, despite having the same values in the short and long time limits.

Figure 7(a) combines the LJ and WCA data from Figs. 6(a) and 6(b) on a single figure. The two curves are symmetric about the $y = x$ line, which is confirmed by rotating them clockwise by $-45°$ and then reflecting the rotated N_-/N_+ curve about the x axis. The curves tracing out the two sets of data in the negative abscissa region are then seen to be statistically indistinguishable. The figure demonstrates that within the simulation statistics, the ratios $-[\eta_-(t)/\eta_+(t)]$ and N_-/N_+ can be made coincident after these two transformations, which suggests that they share the same underlying information. Figure 7(b) presents the property ratios given in the last line of Eq. (10) plotted against each other. The linear trend predicted by the equation is adhered to very well at all times, which supports that analytic treatment.

3. Analytic representations of the PDFs

In Ref. 11, it was shown that P_0 could be represented well by a sum of N_e exponentials (three were employed in that work),

$$P_0(y) = \int_0^\infty H(q)e^{-c_q|y|}\, dq \simeq \sum_{i=1}^{N_e} a_i \exp(-b_i|y|),$$

$$A = \sum_{i=1}^{N_e} \frac{a_i}{b_i^2},$$

(11)

where $H(q)$ is the continuous distribution of decay coefficients, c_q. A discrete sum of exponentials is an approximation to this continuous distribution and has the constants a_i and b_i. Equation (11) also gives a formula for the parameter A, defined in Eq. (10) in terms of the sum of exponentials representation of P_0. The value of A from the formula in Eq. (11) is 0.827(4), which is a little higher than that obtained by directly integrating the simulation PDF. In order to fit to the PDF values smaller than about 0.01, it was found that more exponentials were required, and six were used here. The least squares fit parameters are presented in Table I. The parameters for the sum of exponentials fit to P_0 are sensitive to the dataset used. Nevertheless, the overall fit over the simulated argument range (0–7) is only weakly dependent on the precise MD dataset chosen presumably due to mutual compensation between the terms. The importance of the sum of exponential analytic form of Eq. (11) is that it reproduces the exponential behavior in the tails of the PDF, where the largest viscuits occur.

Figure 8 shows the degree of fit to liquid and solid state points on a lin–lin scale. A stretched exponential ("se") and a Gamma function ("G"),

$$P_{se,0}(y) = A_{se} \exp(-b_{se}y^{\alpha_{se}}),$$

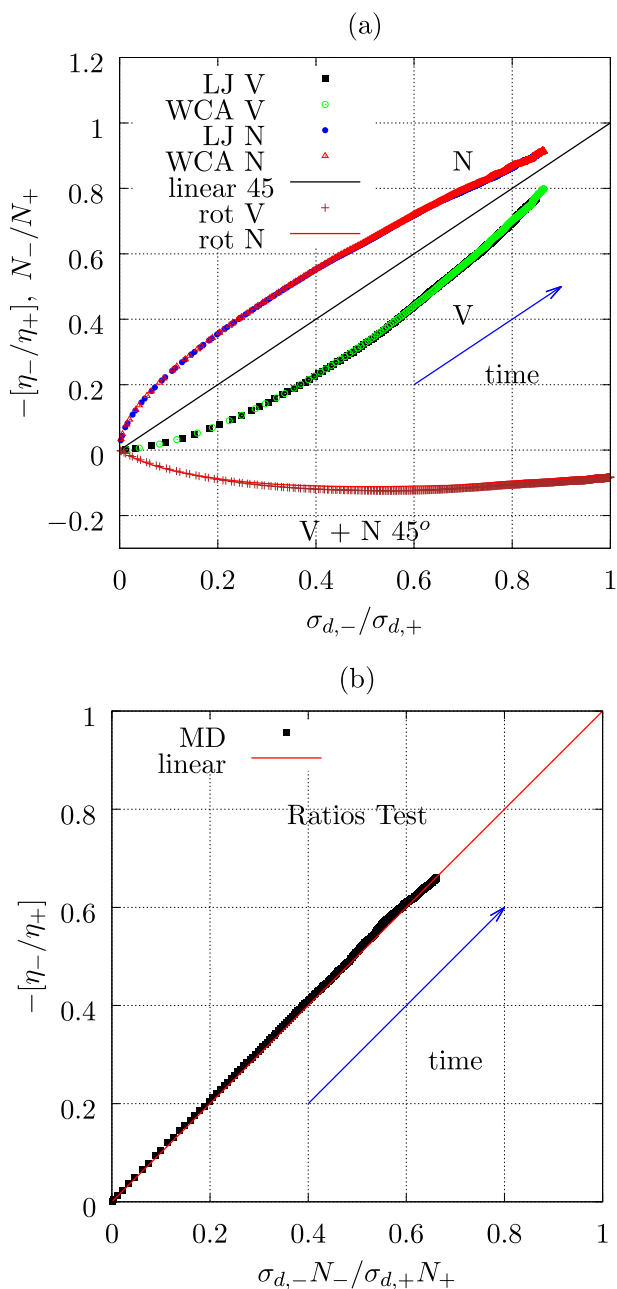$$P_{G,0}(y) = A_G y^{b_G} \exp(-\alpha_G y),$$

(12)

FIG. 7. (a) The LJ and WCA reference state data from Figs. 6(a) and 6(b) combined and rotated clockwise by 45°. The $\eta_-(t)/\eta_+(t)$ and N_-/N_+ are denoted by "V" and "N," respectively, in the figure. In addition, the N_-/N_+ data are then reflected about the x axis. The two sets of data are then coincident within statistics. (b) The property ratios given in the last line of Eq. (10) plotted against each other. The linearity and slope of the data are consistent with the formula for the total viscosity given in that equation.

TABLE I. Least squares fit to the fit formulas for P_0 taking the MD data from that used in Fig. 9(a). Key: a_i and b_i for the sum of exponential formula given in Eq. (11) and the stretched exponential and Gamma function defined in Eq. (12).

quantity		quantity		quantity	
a_1	0.381 159	a_3	0.596 254	a_5	0.058 339
a_2	1.436 787	a_4	0.444 089	a_6	−0.014 486
b_1	0.819 665	b_3	4.034 747	b_5	1.485 265
b_2	15.668 87	b_4	1.485 814	b_6	1.074 376
A_{se}	3.099 582	b_{se}	2.426 957	α_{se}	0.472 958
A_G	0.770 477	b_G	−0.263 138	α_G	0.951 469

Fig. 8. The least squares fit parameters to the analytic expressions in Eq. (12) are also given in Table I. It is perhaps not surprising that they fit quite well as probability distribution functions based on an exponential component are widespread in nature, being associated with "events" that occur independently at a constant average rate.[33,34]

Figure 9(a) shows P_0 on a lin–log scale to focus on the tail region of the viscuits, which cannot be discerned in Fig. 8. Figure 9(a) reveals that while the sum of six exponentials fits the MD data well down to 0.001, the stretched exponential increasingly overestimates the MD data below $P_0 = 0.1$. The Gamma function underestimates the MD data below about $P_0 = 0.04$. The stretched exponential can be expressed as a weighted sum of exponentials,[35] but its simple analytic form imposes constraints on the form of this weighting function, which are apparently not compatible with the viscuit PDF obtained directly by MD over its whole range. Figure 9(b) demonstrates that the same trends are evident for four
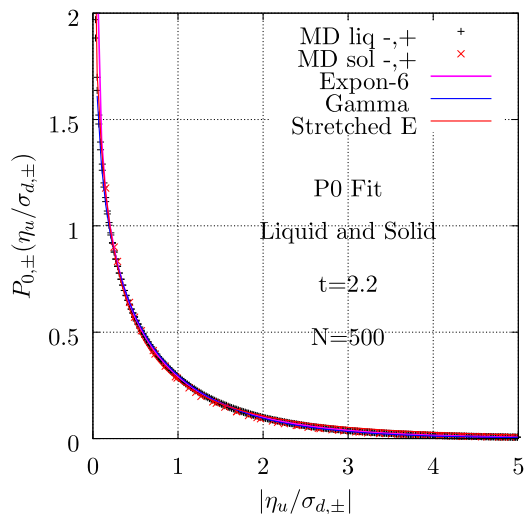
respectively, were also fitted to the MD P_0 data, as they have been used to represent a range of naturally evolving dynamical processes.[31,32] They both agree quite well with the simulation data down to a value of at least 0.1 or $y = 2$, as seen in the lin–lin plot of

FIG. 8. The standard deviation normalized LJ PDFs, P_0, for a liquid, $\rho = 0.8442$ and $T = 0.722$, and solid, $\rho = 1.1$ and $T = 0.8$, state point. The data are plotted on a lin–lin scale. The MD data are shown as symbols, and least square fits to the following functions are as follows: "Expon-6" (sum of 6 exponentials), "Gamma" is a Gamma function, and "Stretched E" is a stretched exponential defined in Eq. (12) as continuous curves.
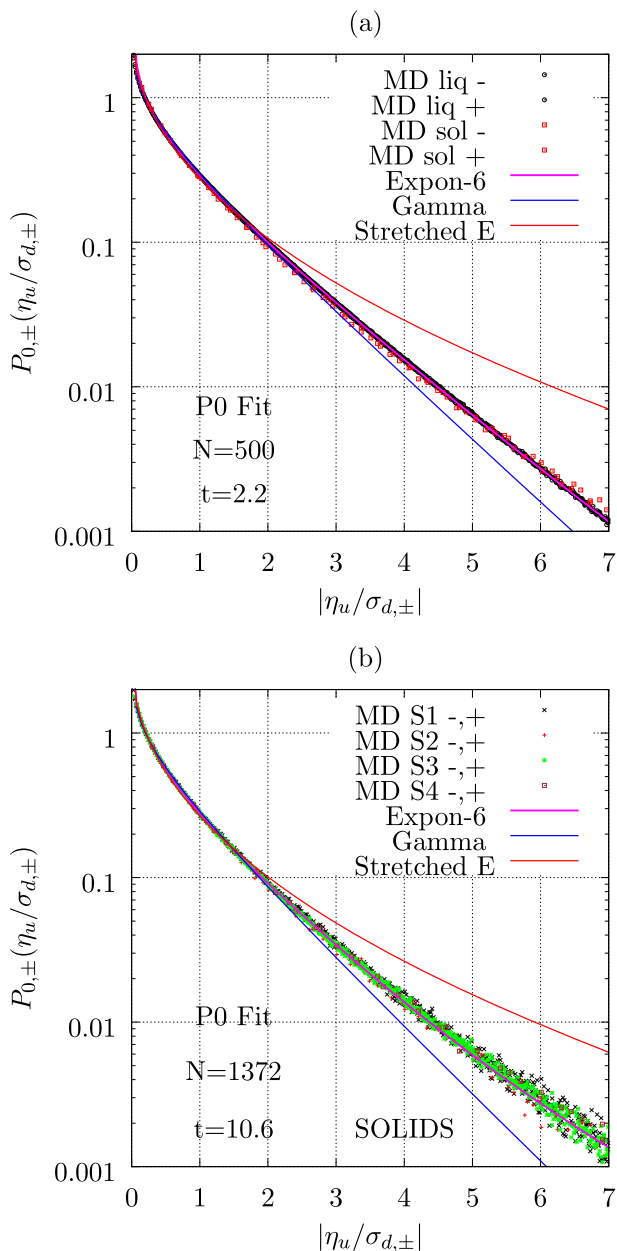
FIG. 9. The standard deviation normalized PDFs, P_0, for LJ state points in the liquid and solid phase shown on a lin–log scale. (a) is for $\rho = 0.8442$ and $T = 0.722$ (liquid) and $\rho = 1.1$ and $T = 0.8$ (solid). (b) is for four solid (ρ, T) state points: 0.9743, 0.578 (S1), 1.3000, 0.578 (S2), 1.0530, 0.2504 (S3), and 1.0670, 0.1670 (S4). S1 and S2 are along an isotherm. S3 and S4 are along the sublimation line (i.e., $P \simeq 0$). Data for both sides of the PDF are plotted separately. The fits over the argument range 0–7 are as follows: "Expon-6" (sum of 6 exponentials), "Gamma" is a Gamma function, and "Stretched E" is a stretched exponential.

solid state points at low temperature and high pressure. The fit is not quite as good as in Fig. 9(a), which may be because these are unusually low temperature and high pressure state points. Nevertheless, this analysis demonstrates the wide range of state points

where the P_0 simplification is practically useful. While P_0 is essentially state point and transport coefficient invariant,[11] the associated standard deviations are generally quite different on the two sides over time scales relevant to the shear viscosity determination [see Fig. 5(a)]. The differences between the two sides of the viscuit PDF are manifest in their standard deviations, calculated for each side separately.

IV. FLUCTUATION THEOREM

Evans, Cohen, and Morriss in 1993[36] gave a general statistical mechanical formula for systems driven out of equilibrium by an external field, which has come to be known as the Fluctuation Theorem (FT) (see also Refs. 37–39). The FT has subsequently been verified by experiment and many NEMD simulations.[40–44] The FT is another route that can be used to derive expressions for positive and negative contributions to the viscosity. The symbols $\eta_{t,-}$ and $\eta_{t,+}$ are given for these FT quantities to distinguish them from the viscuit quantities η_- and η_+.

In the case of shear flow, the external field is the shear rate, $\dot{\gamma}$. The SLLOD NEMD equations of motion can be used to implement homogeneous shear flow,[45] and the quantity of interest for the FT description of this situation is the mean shear stress, σ_t, over time t for a single trajectory,

$$\sigma_t = \frac{1}{t} \int_0^t \sigma(u) \, du. \tag{13}$$

The terms "block average" and "t-average" shear stress are often used for σ_t. Note that in the viscuit treatment of Sec. III, the PDF is that of viscuits, which are time integrals of the product of two instantaneous stresses at different times. The PDF in the FT case is of the t−average shear stress. Although the two quantities are not the same, they are related, but it would appear, not in a particularly trivial way, as will be discussed below. The PDF of σ_t is denoted by $P_t(\sigma_t)$, where the t subscript emphasizes that its functional form can depend on the sampling time, t. The t-average PDF extends over all the negative and positive values of σ_t and is characterized by a single standard deviation. There does not appear to be an obvious advantage in separating the FT PDF into two different functions on the two sides, unlike in the viscuit case.

For $t > \tau_s$ [the relaxation time, see Eq. (2)], as evident in Fig. 6 of Ref. 38, the PDF of σ_t *tends to* a shifted Gaussian, irrespective of the shear rate,

$$P_t(\sigma_t) = \frac{1}{\sqrt{2\pi}\sigma_{d,t}} \exp\left(-\frac{(\sigma_t - \overline{\sigma}_t)^2}{2\sigma_{d,t}^2}\right) = \frac{1}{\sqrt{2\pi}\sigma_{d,t}}$$
$$\times \exp\left(-\frac{\delta\sigma_t^2}{2\sigma_{d,t}^2}\right), \quad \delta\sigma_t = \sigma_t - \overline{\sigma}_t, \ \sigma_{d,t}^2 \equiv \langle \delta\sigma_t^2 \rangle, \tag{14}$$

where the simulation average, $\overline{\sigma}_t \geq 0$ (for $\dot{\gamma} > 0$), is the average of σ_t over the entire time domain covered for large t. The standard deviation of these block averages is $\sigma_{d,t}$, which is determined for the whole t-average range, $-\infty < \sigma_t < \infty$. The two parts of the PDF relevant to the FT are

$$P_t(\sigma_t) = \frac{1}{\sqrt{2\pi}\sigma_{d,t}} \exp\left(-\frac{(\sigma_t - \overline{\sigma}_t)^2}{2\sigma_{d,t}^2}\right),$$

$$P_t(-\sigma_t) = \frac{1}{\sqrt{2\pi}\sigma_{d,t}} \exp\left(-\frac{(-\sigma_t - \overline{\sigma}_t)^2}{2\sigma_{d,t}^2}\right). \tag{15}$$

For the FT, the ratio of these two PDFs is required.[38,39] The two expressions in Eq. (15) combined give

$$\frac{P_t(\sigma_t)}{P_t(-\sigma_t)} = \exp\left(2\frac{\sigma_t\overline{\sigma}_t}{\sigma_{d,t}^2}\right). \tag{16}$$

The FT term on the right-hand side is[39]

$$\frac{P_t(\sigma_t)}{P_t(-\sigma_t)} = \exp(V\sigma_t\dot{\gamma}t\beta), \tag{17}$$

where V is the volume, $\dot{\gamma}$ is the (constant) steady state shear rate, $\beta = 1/k_BT$, and k_B is Boltzmann's constant. For the shifted Gaussian PDF to satisfy the FT, it requires that

$$2\frac{\overline{\sigma}_t}{\sigma_{d,t}^2} = V\dot{\gamma}t\beta. \tag{18}$$

It was proved by Searles and Evans[39] that the GK and EHK expressions for transport coefficients can be derived using the FT assuming a Gaussian distribution for the t−averaged stress (in the case of the viscosity) taking the $t \to \infty$ limit and providing that the system is close to equilibrium (i.e., $\dot{\gamma} \ll 1$, in LJ reduced units). The usual GK expression can be applied in these circumstances, provided $\sigma(t)$ is replaced by $\delta\sigma(t) = \sigma(t) - \overline{\sigma}$, the excess stress from the mean. The shear viscosity is $\eta(\dot{\gamma}) = G_{\infty,0}(\dot{\gamma})\tau_s(\dot{\gamma})$, where τ_s is the relaxation time, and if $\delta\sigma_0 \equiv \delta\sigma(0)$, the infinite frequency shear modulus is $G_{\infty,0} = \langle\delta\sigma_0^2\rangle V\beta$,

$$\tau_s = \int_0^\infty \frac{\langle\delta\sigma(0)\delta\sigma(x)\rangle}{\langle\delta\sigma_0^2\rangle}dx, \quad s = 2\tau_s. \tag{19}$$

Therefore, from Eqs. (18) and (19),

$$\overline{\sigma}_t = \frac{\sigma_{d,t}^2}{2}V\dot{\gamma}t\beta = s\frac{\langle\delta\sigma_0^2\rangle}{2}V\dot{\gamma}\beta$$

$$= \tau_s\langle\delta\sigma_0^2\rangle V\dot{\gamma}\beta = G_{\infty,0}\tau_s\dot{\gamma} = \eta\dot{\gamma}, \tag{20}$$

which uses the Gaussian statistics relationship that $\sigma_{d,t}^2 = [s/t]\langle\sigma_0^2\rangle$. Equation (20) proves that the shifted Gaussian is consistent with the FT. This is applicable in the large t limit and weak field regime (i.e., here, $\dot{\gamma} \to 0$) because the PDF is no longer a shifted Gaussian (particularly in the wings) at high shear rates. The FT does not require the PDF to be a shifted Gaussian, though.

The shifted Gaussian expression for the t-average PDF defined in Eq. (14) can be employed to derive approximate analytic expressions for certain quantities, which can also be readily computed in an NEMD simulation. Figure 10 shows the σ_t probability distribution function at the state point $\rho = 0.8442$ and $T = 0.722$ using the WCA potential for a shear rate of $\dot{\gamma} = 0.025$ for three values of the averaging time, t. The figure shows that the PDF departs from the Gaussian for the three t-cases. They are skewed and exhibit an extended tail on the
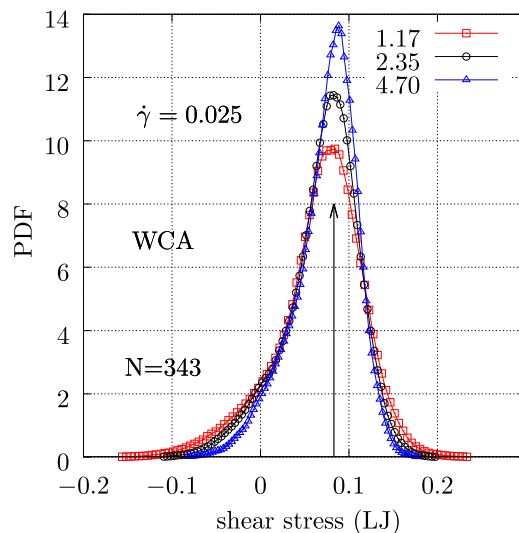

FIG. 10. The shear stress t-average [see Eq. (13)] probability distribution function, which is relevant to the fluctuation theorem. The key parameters are $\rho = 0.8442$, $T = 0.722$, $N = 256$, and $\dot{\gamma} = 0.025$. The WCA potential was used in the NEMD SLLOD simulations. The t values used to define the t-averages are given in the figure. Data for three values of t are considered.

negative side. At this near triple point state point, there are departures from a Gaussian t-average PDF even at quite small shear rates. The mean stress is therefore less than the peak value. Equation (23) gives for the FT

$$\lim_{t\to\infty} \frac{1}{t}\ln\left(\frac{P_t(\sigma_t)}{P_t(-\sigma_t)}\right) = V\dot{\gamma}\beta\sigma_t, \tag{21}$$

where $\sigma_t \geq 0$, which is confirmed within the MD statistics in Fig. 11 for data from the current NEMD simulations.

A. Number ratio of t-averages on the two sides

The relative number of positive and negative occurrences of the t-averaged stress, σ_t, over a simulation is $N_{t,+}/N_{t,-}$, where $N_{t,+}$ is the number of t-averages, σ_t, which are positive and $N_{t,-}$ is the number of negative occurrences of σ_t. These two quantities can be computed directly during the simulation as a function of t and $\dot{\gamma}$. The FT was used by Evans and Searles in Ref. 39 to derive an expression for $N_{t,+}/N_{t,-}$ as a function of t whose steps in the present notation are

$$\frac{N_{t,+}}{N_{t,-}} = \frac{\int_0^\infty P_t(\sigma_t)\,d\sigma_t}{\int_{-\infty}^0 P_t(\sigma_t)\,d\sigma_t}$$

$$= \frac{\int_0^\infty P_t(\sigma_t)\,d\sigma_t}{\int_0^\infty P_t(-\sigma_t)\,d\sigma_t}. \tag{22}$$

Equation (22) is valid because the PDF is defined over the whole t-average range. According to the FT,
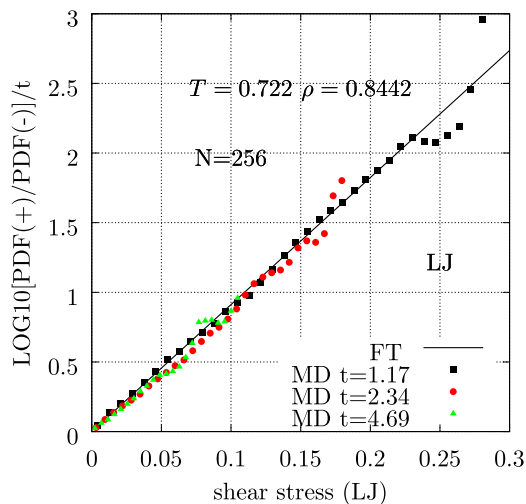
FIG. 11. Validation of the fluctuation theorem as written in the form of Eq. (21) involving the ratio of the two sides of the t-average stress PDF using the SLLOD NEMD data of this work. The system simulation parameters are ρ = 0.8442, T = 0.722, and N = 256. The PDF ratio is plotted against the average shear stress, σ_t, which increases with the shear rate. Data for three values of t are shown. The WCA potential was used, and the simulation was for 2940 LJ time units. Note that the black line is *not* a fit to the MD data (symbols) but that predicted by the FT (i.e., the slope is $V\dot{\gamma}\beta$).

$$P_t(\sigma_t) = e^{B\sigma_t t} P_t(-\sigma_t),$$
$$P_t(-\sigma_t) = e^{-B\sigma_t t} P_t(\sigma_t), \tag{23}$$

where $B = V\dot{\gamma}/k_B T$ and $\sigma_t \geq 0$. Substituting the formulas in Eq. (23) in Eq. (22) gives

$$\frac{N_{t,+}}{N_{t,-}} = \frac{\int_0^\infty e^{B\sigma_t t} P_t(-\sigma_t)\, d\sigma_t}{\int_0^\infty P_t(-\sigma_t)\, d\sigma_t} \equiv \langle e^{B\sigma_t t} \rangle_-,$$
$$\frac{N_{t,+}}{N_{t,-}} = \frac{\int_0^\infty P_t(\sigma_t)\, d\sigma_t}{\int_0^\infty e^{-B\sigma_t t} P_t(\sigma_t)\, d\sigma_t} \equiv \langle e^{-B\sigma_t t} \rangle_+^{-1}, \tag{24}$$

where $\langle \cdots \rangle_\pm$ denotes a simulation average in either the negative or positive stress sides of the t-average stress PDF. The averages on the negative stress (i.e., $-\sigma_t$) side are signified by $\langle \cdots \rangle_-$. In any practical application, the condition

$$1 = \langle e^{B\sigma_t t} \rangle_- \langle e^{-B\sigma_t t} \rangle_+ \tag{25}$$

follows directly from Eq. (24), which acts as a useful measure of the sampling efficiency of these quantities during and NEMD simulation. One might expect the statistical errors on the first formula of Eq. (24) for $N_{t,+}/N_{t,-}$ to be larger than the second because as the shear rate increases, relatively fewer states with a negative stress will appear because the PDF is shifted to the right, as has already been noted in Ref. 39. Therefore, the first condition in Eq. (24) should suffer from sampling limitations for finite duration simulations. Large contributors to both averages in Eq. (24) will be dominated by quite rare events. In the case of the negative stress t-average, those states

with large negative values will dominate the right-hand sides of the first formula in Eq. (24). In the case of the positive stress t-average, those states when the stress is small will dominate.

Following on from Eq. (22), the fraction of t-averages with negative and positive values are

$$\frac{N_{t,-}}{N_{t,+} + N_{t,-}} = \frac{\langle e^{-B\sigma_t t} \rangle_+}{1 + \langle e^{-B\sigma_t t} \rangle_+} \equiv \frac{1}{1 + \langle e^{+B\sigma_t t} \rangle_-},$$
$$\frac{N_{t,+}}{N_{t,+} + N_{t,-}} = \frac{\langle e^{B\sigma_t t} \rangle_-}{1 + \langle e^{B\sigma_t t} \rangle_-} \equiv \frac{1}{1 + \langle e^{-B\sigma_t t} \rangle_+}. \tag{26}$$

Note that $\sigma_t \geq 0$ in Eq. (26), which follows from the definitions in Eqs. (22)–(24). The FT-predicted quantities in Eqs. (22) and (26) can be compared with the same quantities computed directly and independently during an NEMD simulation.

Assuming a shifted Gaussian σ_t PDF for all t, an analytic expression for $N_{t,+}/N_{t,-}$ can be derived by variable substitution and integration, which is

$$\frac{N_{t,+}}{N_{t,-}} = \frac{\int_0^\infty \exp\left(-\frac{(x_t - \bar{x}_t)^2}{2}\right) dx_t}{\int_{-\infty}^0 \exp\left(-\frac{(x_t - \bar{x}_t)^2}{2}\right) dx_t}$$
$$= \frac{1 + erf(\bar{x}_t/\sqrt{2})}{1 - erf(\bar{x}_t/\sqrt{2})}, \tag{27}$$

where $x_t = \sigma_t/\sigma_{d,t}$, erf is the error function, and $\bar{x}_t = \langle x_t \rangle = \langle \sigma_t \rangle/\sigma_{d,t}$.

Figure 12(a) presents the ratio of the number of positive to negative t-averaged stress states, $N_{t,+}/N_{t,-}$, as a function of shear rate for three values of t. This ratio is expected to increase with time, t, for a given value of $\dot{\gamma}$. The ratio $N_{t,+}/N_{t,-}$ increases with the shear rate for a given t because the PDF then shifts more into the positive stress side. The prediction by the shifted Gaussian approximation for the shear stress PDF given in Eq. (27) agrees very well with the values computed directly by NEMD in the range up to $\dot{\gamma} \leq 0.15$ at least, as may be seen in Fig. 12(a). This is the case even though the PDFs may show noticeable departures from the Gaussian form. This is the case even at relatively small shear rates at the reference state point, as seen in Fig. 10, for which $\dot{\gamma}$ = 0.025. The relative number of positive to negative t-averages on the two sides appears not to be too sensitive to the skewness of the PDF presumably because of cancellation of the contributions in different stress ranges because of the extent and height of the tail in the wings on the two sides.

Figure 12(b) shows the curves compared with the FT predictions given in Eq. (24) for t = 0.288. The formula in the first line of Eq. (24) involves an average computed from the negative stress states, while the second formula in the equation is an average over the positive stress states. The second formula agrees best with the MD values but still systematically underestimates the exact values. The first formula in Eq. (24) to a greater extent underestimates the correct values, which is expected as discussed above. The magnitude of this sampling deficiency was also pointed out in Ref. 39 (p. 1562) for the negative side sampling statistics.

B. Ratio of ± contributions to the viscosity

The average shear stress, broken up into its negative and positive value contributions, can be expressed in terms of the first moment of the σ_t PDF as
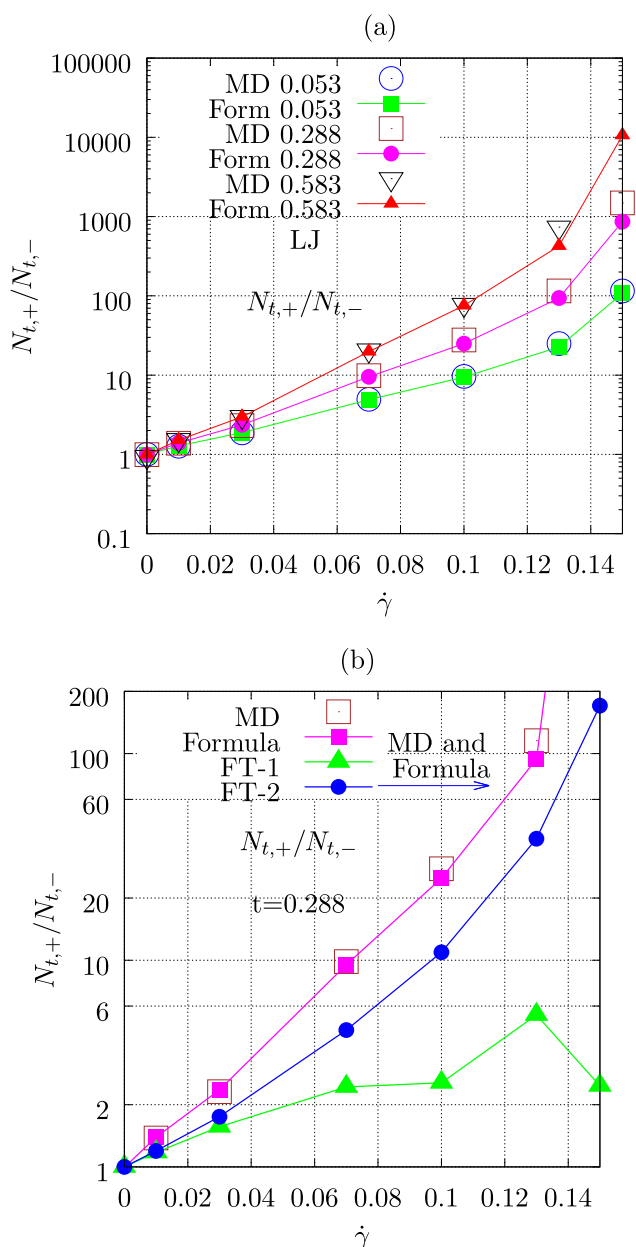
FIG. 12. The ratio of the number of positive to negative t-averaged stress states, N_+/N_-, as a function of shear rate for the $\rho = 0.8442$ and $T = 0.722$ state point using the LJ potential with $N = 256$. (a) Three t-average times are considered with their values given in the figure. The ratios computed directly by MD are compared with the predictions of the analytic formula given in Eq. (27). (b) presents the $t = 0.288$ data from (a) and compares it with the FT predictions given in Eq. (24). The formula in the first line of Eq. (24) is denoted in the figure by "FT-1," and the formula on the second line is "FT-2."

$$\overline{\sigma}_t = \overline{\sigma}_{t,-} + \overline{\sigma}_{t,+}$$

$$= \int_{-\infty}^{0} \sigma_t P_t(\sigma_t) d\sigma_t + \int_{0}^{\infty} \sigma_t P_t(\sigma_t) d\sigma_t, \quad (28)$$

where $\overline{\sigma}_{t,-} < 0$ and $\overline{\sigma}_{t,+} > 0$. Note that the PDF in Eq. (28) extends over the entire negative and positive stress sides and

is defined in terms of a single standard deviation, which is t-dependent.

Substituting Eq. (14) into Eq. (28) after rearrangement and integration gives

$$\frac{\overline{\sigma}_{t,-}}{\sigma_{d,t}} = -\frac{\exp(-\overline{x}_t^2/2)}{\sqrt{2\pi}} + \frac{\overline{x}_t}{2}\left(1 - erf\left(\frac{\overline{x}_t}{\sqrt{2}}\right)\right),$$

$$\frac{\overline{\sigma}_{t,+}}{\sigma_{d,t}} = \frac{\exp(-\overline{x}_t^2/2)}{\sqrt{2\pi}} + \frac{\overline{x}_t}{2}\left(1 + erf\left(\frac{\overline{x}_t}{\sqrt{2}}\right)\right), \quad \overline{\sigma}_{t,-} + \overline{\sigma}_{t,+} = \overline{\sigma}_t, \quad (29)$$

where $x_t = \sigma_t/\sigma_{d,t}$. The last line of Eq. (29) is the sum of the first two lines. The simulation time average, $\overline{x}_t$, is the average of x_t that depends on time because of the time dependence of $\sigma_{d,t}$ (which is finite for all t). The shear rate also has an effect on $\overline{x}_t$. For large t, $\sigma_{d,t}$ will scale as $\propto t^{1/2}$.

As the standard deviation $\sigma_{d,t}$ is amassed from *both* sides of the PDF and the shear rate is common to both sides, the ratio of the positive to negative contributions to the viscosity $\eta_{t,+}/\eta_{t,-} = \overline{\sigma}_{t,+}/\overline{\sigma}_{t,-}$ in the shifted Gaussian approximation follows from Eq. (29) and is

$$\frac{\eta_{t,+}}{\eta_{t,-}} = \frac{\frac{\exp(-\overline{x}_t^2/2)}{\sqrt{2\pi}} + \frac{\overline{x}_t}{2}\left(1 + erf\left(\frac{\overline{x}_t}{\sqrt{2}}\right)\right)}{-\frac{\exp(-\overline{x}_t^2/2)}{\sqrt{2\pi}} + \frac{\overline{x}_t}{2}\left(1 - erf\left(\frac{\overline{x}_t}{\sqrt{2}}\right)\right)}. \quad (30)$$

Note that this ratio is negative as $\eta_- < 0$. Equation (30) leads to

$$\lim_{\overline{x}_t \to 0}\left(\frac{\eta_{t,+}}{\eta_{t,-}}\right) = \frac{\left[\frac{1}{\sqrt{2\pi}}\right] + \frac{\overline{x}_t}{2} + \frac{\overline{x}_t^2}{2\sqrt{2\pi}} + O(\overline{x}_t^3)}{-\left[\frac{1}{\sqrt{2\pi}}\right] + \frac{\overline{x}_t}{2} - \frac{\overline{x}_t^2}{2\sqrt{2\pi}} + O(\overline{x}_t^3)},$$

$$\lim_{\dot{\gamma} \to 0}(\eta_{t,-} + \eta_{t,+}) = \eta_t, \quad (31)$$

where the last line follows directly from Eq. (29). In the limits $\dot{\gamma} \to 0$ and hence $\overline{x}_t \to 0$, $\eta_{t,+}/\eta_{t,+} \to -1$. The contributions of $\eta_{t,-}$ and $\eta_{t,+}$ to the total viscosity are equal in the zero shear rate limit, whereas this is not the case for the viscuit-derived quantities η_- and η_+. Figure 13 compares $-\eta_{t,+}/\eta_{t,-}$ obtained directly by NEMD and the shifted-Gaussian approximation given in Eq. (30) for three t-averaging times. The same parameters as Fig. 12 are used. The agreement is very good, despite the PDFs departing from a Gaussian shape under shear for the values of t given in the figure.

Each single trajectory or segment leading to a particular $\delta\sigma_t^2$ can be written in terms of a sum of t viscuits (treating t to be an integer number of time increments or steps in a simulation) of duration 0 to t. In fact, in principle, for large enough t, one would only need a single segment to have sufficient averaging to determine the viscosity (i.e., is tantamount to the EHK method). The viscuit, $\eta_u(t)$, is a component of any single $\delta\sigma_t^2$. Searles and Evans proved the (generalized) Einstein–Helfand–Kubo[16,46,47] and Green–Kubo formulas for the shear viscosity for small but not zero shear rate and for large $t \to \infty$,

$$\langle(\sigma_t - \overline{\sigma})^2\rangle \equiv \langle\delta\sigma_t^2\rangle = \frac{2}{t}\int_0^t \langle\delta\sigma(0)\delta\sigma(t')\rangle dt', \quad (32)$$
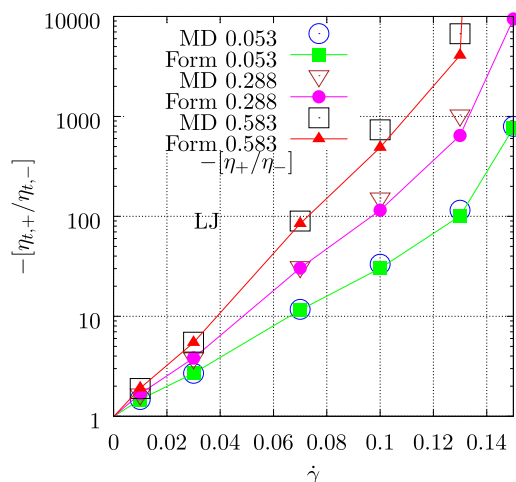
whereas for a single trajectory,

FIG. 13. As for Fig. 12, except $-\eta_+/\eta_-$ is plotted. Again the values obtained directly from the MD simulations and the shifted-Gaussian approximation of Eq. (30) are compared for three t stress-averaging times.

$$(\sigma_t - \overline{\sigma})^2 \simeq \frac{2}{t} \sum_{k=1}^{t} \sum_{k'=k}^{t} \delta\sigma(k)\delta\sigma(k')\Delta t', \qquad (33)$$

where $\Delta t'$ is a time interval such as a simulation time step. The double summation indicates that the *single* $\delta\sigma_t^2$ contains a sum of viscuits of time length from 0 to t. It is therefore valid to state that the viscuit analysis is related to the FT (in the limit $\dot{\gamma} \to 0$) but currently not in an obviously tractable way to link the two approaches in all aspects.

V. CONCLUSIONS

The viscuit reformulation of the Green–Kubo (GK) method for the shear viscosity has the useful feature that the shear stress relaxation "events," which give rise to the viscosity, η, can be resolved into those that make negative and positive contributions to η, a feature that is at the center of this work. This separation reveals clearly the role played by "noise" in the time correlation functions, whose time dependence can be exploited to evaluate the viscosity. These positive and negative contributions to the viscosity are present even for purely repulsive pair potential systems.

Traditional use of Green–Kubo (GK) has been hampered by statistical uncertainty in the integral of the stress autocorrelation function in a time range where a plateau is expected. This is due to finite simulation lengths that are inevitable in practice. A reformulation of GK in terms of its component elements or "viscuits" carried out here leads to three new definitions of the (Newtonian) viscosity in terms of the viscuit formulation, two of which involve its probability distribution function (PDF). These can be computed readily in an equilibrium Molecular Dynamics (MD) simulation.

These three new methods, to varying extents, exploit the time region where the noise becomes increasingly important and beyond the correlation time of the shear stress autocorrelation function. Equation (6) involves extrapolating to zero time the negative and

positive average viscuit GK component from well within the noise-dominated time regime. The viscosity is simply the sum of the two intercepts. This relies on obtaining very good statistics for the time dependence of the negative and positive viscuit contributions to the viscosity in the large time limit. This is possible for the simple model systems treated in this work. It may be more problematic for more complex molecules where exploration of phase space is a more computationally demanding task.

Equation (7) presents the second method, which uses the difference in the PDF on the negative and positive viscuit sides at the same magnitude of the viscuit. The PDF employed is evaluated over the whole viscuit domain. The third new method defined in Eq. (10) makes use of statistical properties of the two sides of the PDF treated separately. This third method formula relies on obtaining two quantities of the two negative and positive quadrants. It also requires assignment of a basic constant, A, which also has (currently) to be obtained numerically. As a result, this method probably exhibits the largest statistical uncertainty when employed in MD. This formula might prove useful nevertheless if these characteristic quantities could be obtained approximately by theory without resort to MD simulation.

Of the three viscuit routes to η, the second one defined in Eq. (7) might have the most significant practical benefit in simulations. It is straightforward to implement and gives a plateau, which is largely free of noise, and therefore helps assign a well-defined value for the viscosity. It does not reduce the necessary total run simulation time compared to the original GK method, however, because the plateau value is a function of the total simulation length and follows broadly the GK plateau value (which is however much noisier) at each simulation length. This is not surprising in retrospect as the two approaches use the same starting information. For a sufficiently long simulation time, this PDF route may possibly remove the "plateau problem," which would enable a more precise value of the viscosity to be determined by equilibrium MD. A more systematic MD investigation would be required to see if this is the case, however. Another advantage of the PDF route to the viscosity is that many statistical mechanical theories of the liquid state are based on a presumed distribution of dynamical events, which, for example, may represent "hopping" of the system between local basins of attraction.[48] The PDF viscuit reformulation of GK would naturally be compatible with such a formulation and therefore help explore and test these theories.

An outstanding challenge is how to assign physically meaningful positive and negative viscuit contributions to the viscosity, which may have statistical mechanical significance. It might be considered that these two numbers should be unique as physical quantities, but their values increase dramatically with the time ascribed to the plateau value in the Green–Kubo integral and formally equivalent viscuit PDF routes. They are very sensitive to the precise value of the cutoff time, t, which is used to assign the viscosity in the plateau region. An objective criterion to assign these two numbers would be a useful advance.

Along an isomorph, the viscuit PDF should exhibit isomorph scaling when the stress is divided by ρT. The current evidence is, however, that the liquid–solid melting and freezing lines are not isomorphs in the vicinity of the triple point.[49,50] The principal state point used here $\rho = 0.8442$ and $T = 0.722$ is close to the triple point, so the status of isomorph scaling in this region is still unresolved.

10 June 2024 11:11:24

However, if a simulation were to be carried out at a temperature of above about 2.0 along the freezing line, then very good isomorph scaling should be observed in the viscuit PDFs. The extension of the present MD viscuit analysis to molecular fluids would be a promising future direction. As the theory makes no specific reference to molecular type, it should be applicable also to polyatomic molecules in just the same way as for the Lennard-Jones system. The qualitative features should be the same, but there may be systematic quantitative differences as the molecules become more complex. The role of intramolecular interactions and chain length in organic molecules would be aspects that could be studied.

Further practical applications of the Fluctuation Theorem (FT) are considered in this study, as negative and positive contributions to the viscosity are also a feature of the FT treatment. Approximate analytic expressions for the relative number of positive to negative block average shear stresses are derived assuming a shifted Gaussian PDF in the FT approach. Some of these are shown to agree well with non-equilibrium molecular dynamics simulations, despite the fact that the PDFs exhibit non-negligible departures from a shifted Gaussian in the cases investigated here. This indicates a cancellation of certain processes, which may be worth further investigation. A similar treatment of the positive and negative block average contributions to the viscosity is also shown to reproduce the simulation data remarkably well.

There is a qualitative difference between the analytic forms of the PDFs in the viscuit analysis compared to those typically encountered with the FT. These have near exponential and (typically) Gaussian reference forms, respectively. The viscuit could be viewed to be a dynamical "event" originating at the molecular level, which occurs essentially randomly in time (but having a well-defined average occurrence frequency depending on magnitude). The viscuit might consequently be expected to exhibit an exponential distribution, at least over part of its range. Another example of a dynamical event originating on the molecular scale is the net force on a molecule in a liquid, which also has been found to have an exponential or near exponential distribution for some state points.[51,52]

The Green–Kubo method has become a widely employed tool in determining the viscosity of practically relevant liquids, for example, in tribology.[53] These new ways of obtaining the viscosity from the viscuit reformulation of GK derived here may find use in that field.

SUPPLEMENTARY MATERIAL

The supplementary material contains the MD simulation determined time correlation function and time-dependent viscosity data used to generate Figs. 1 and 2. This is for the R1 state point. In addition, the simulations that produced the data for Figs. 1, 2, 4, and 5 in this paper are repeated with MD data generated at the R2 state point, $\rho = 0.8$ and $T = 1.0$. The corresponding figures for this state point are also shown.

ACKNOWLEDGMENTS

DATA AVAILABILITY

The data that support the findings of this study are available upon reasonable request from the corresponding author or at tribology@imperial.ac.uk.

REFERENCES

[1] J.-P. Hansen and I. R. McDonald, *Theory of Simple Liquids*, 4th ed. (Academic Press, Amsterdam, 2013).
[2] D. Levesque, L. Verlet, and J. Kürkijarvi, Phys. Rev. A **7**, 1690 (1973).
[3] R. Zwanzig and N. K. Ailawadi, Phys. Rev. **182**, 280 (1969).
[4] I. Bitsanis, M. Tirrell, and H. T. Davis, Phys. Rev. A **36**, 958 (1987).
[5] R. E. Jones and K. K. Mandadapu, J. Chem. Phys. **136**, 154102 (2012).
[6] Y. Zhang, A. Otani, and E. J. Maginn, J. Chem. Theory Comput. **11**, 3537 (2015).
[7] C. Kim, O. Borodin, and G. E. Karniadakis, J. Comput. Phys. **302**, 485 (2015).
[8] K.-S. Kim, M. H. Han, C. Kim, Z. Li, G. E. Karniadakis, and E. K. Lee, J. Chem. Phys. **149**, 044510 (2018).
[9] D. Nevins and F. J. Spera, Mol. Simul. **33**, 1261 (2007).
[10] D. M. Heyes, E. R. Smith, and D. Dini, J. Chem. Phys. **150**, 174504 (2019).
[11] D. M. Heyes, D. Dini, and E. R. Smith, J. Chem. Phys. **152**, 194504 (2020).
[12] D. M. Heyes, D. Dini, and E. R. Smith, Phys. Status Solidi B **257**, 2000344 (2020).
[13] J. C. Maxwell, Philos. Trans. R. Soc. London **157**, 49 (1867).
[14] R. Hartkamp, P. J. Daivis, and B. D. Todd, Phys. Rev. E **87**, 032155 (2013).
[15] F. H. Stillinger and P. G. Debenedetti, J. Phys. Chem. B **109**, 6604 (2005).
[16] J. J. Erpenbeck, Phys. Rev. E **51**, 4296 (1995).
[17] There is an error in the third line of Eq. (15) in Ref. 10. The correct formula was used in the simulations of that reference, and is given in Eq. (4) of this work.
[18] D. Levesque and L. Verlet, Phys. Rev. A **2**, 2514 (1970).
[19] D. Levesque and L. Verlet, Mol. Phys. **61**, 143 (1987).
[20] A. J. Schultz and D. A. Kofke, J. Chem. Phys. **149**, 204508 (2018).
[21] L. V. Woodcock, AIChE J. **52**, 438 (2006).
[22] K. Meier, A. Laesecke, and S. Kabelac, J. Chem. Phys. **121**, 3671 (2004).
[23] J. D. Weeks, D. Chandler, and H. C. Andersen, J. Chem. Phys. **54**, 5237 (1971).
[24] A. Ahmed and R. J. Sadus, Phys. Rev. E **80**, 061101 (2009).
[25] W. G. Hoover, Phys. Rev. A **31**, 1695 (1985).
[26] D. J. Evans and G. P. Morriss, Phys. Rev. A **30**, 1528 (1984).
[27] A. J. C. Ladd, Mol. Phys. **53**, 459 (1984).
[28] L. de Sousa Oliveira and P. A. Greaney, J. Chem. Phys. **95**, 023308 (2017).
[29] M. Wallner, Eur. J. Comb. **87**, 103138 (2020).
[30] S. R. Williams and D. J. Evans, J. Chem. Phys. **131**, 024115 (2009).
[31] J. C. Phillips, Rep. Prog. Phys. **59**, 1133 (1996).
[32] J. G. Powles, D. M. Heyes, G. Rickayzen, and W. A. B. Evans, J. Chem. Phys. **131**, 214509 (2009).
[33] H. Touchette, Phys. Rep. **478**, 1 (2009).
[34] M. O. Vlad, D. L. Huber, and J. Ross, J. Chem. Phys. **106**, 4157 (1997).
[35] C. P. Lindsey and G. D. Patterson, J. Chem. Phys. **73**, 003348 (2008).
[36] D. J. Evans, E. G. D. Cohen, and G. P. Morriss, Phys. Rev. Lett. **71**, 2401 (1993).
[37] D. J. Evans and G. P. Morriss, Phys. Rev. A **38**, 4142 (1988).
[38] D. J. Searles and D. J. Evans, J. Chem. Phys. **112**, 9727 (2000).
[39] D. J. Evans and D. J. Searles, Adv. Phys. **51**, 1529 (2002).
[40] G. Ayton, D. J. Evans, and D. J. Searles, J. Chem. Phys. **115**, 2033 (2000).
[41] D. J. Evans, D. J. Searles, and E. Mittag, Phys. Rev. E **63**, 051105 (2001).
[42] D. J. Searles and D. J. Evans, Int. J. Thermophys. **22**, 123 (2001).
[43] S. R. Williams, D. J. Searles, and D. J. Evans, J. Chem. Phys. **124**, 194102 (2006).
[44] E. Mittag and D. J. Evans, Phys. Rev. E **67**, 026113 (2003).
[45] D. J. Evans and G. Morriss, *Statistical Mechanics of Nonequilibrium Liquidsliquids*, 2nd ed. (Cambridge University Press, Cambridge, 2008).
[46] S. Hess and D. J. Evans, Phys. Rev. E **64**, 011207 (2001).
[47] E. Helfand, Phys. Rev. **119**, 1 (1960).
[48] J. D. Gezelter, E. Rabani, and B. J. Berne, J. Chem. Phys. **107**, 4618 (1997).

10 June 2024 11:11:24

[49] D. M. Heyes and A. C. Brańka, J. Chem. Phys. **143**, 234504 (2015).

[50] U. R. Pedersen, L. Costigliola, N. P. Bailey, T. B. Schrøder, and J. C. Dyre, Nat. Commun. **7**, 12386 (2016).

[51] J. G. Powles and R. F. Fowler, Mol. Phys. **62**, 1079 (1987).

[52] G. Rickayzen, A. C. Brańka, S. Pieprzyk, and D. M. Heyes, J. Chem. Phys. **137**, 094505 (2012).

[53] N. D. Kondratyuk, V. V. Pisarev, and J. P. Ewen, J. Chem. Phys. **153**, 154502 (2020).

10 June 2024 11:11:24